J. Fluid Mech. (1989), *vol.* 207, *pp.* 419–452
Printed in Great Britain

Spectra and energy transfer in stably stratified turbulence

By E. C. ITSWEIRE[1] AND K. N. HELLAND[2]†

[1] Chesapeake Bay Institute, The Johns Hopkins University, Baltimore, MD 21211, USA

[2] Institute for Pure and Applied Physical Sciences, University of California, San Diego, La Jolla CA 92093, USA

(Received 20 September 1988 and in revised form 4 April 1989)

The influence of stabilizing buoyancy forces on the spectral characteristics and spectral energy transfer of grid-generated turbulence was studied in a ten-layer closed-loop stratified water channel. The results are compared to the limiting ideal cases of the three-dimensional turbulence and two-dimensional turbulence theories. The velocity power spectra evolve from a classical isotropic shape to a shape of almost k^{-2} after the suppression of the net vertical mixing. This final spectral shape is rather different from the k^{-3} to k^{-4} predicted by the theory of two-dimensional turbulence and could result from the interaction between small-scale internal waves and quasi-two-dimensional turbulent structures as well as some Doppler shift of advected waves. Several lengthscales are derived from the cospectra of the vertical velocity and density fluctuations and compared with the buoyancy, overturning and viscous lengthscales measured in previous studies, e.g. Stillinger, Helland & Van Atta (1983) and Itsweire, Helland & Van Atta (1986). The smallest turbulent scale, defined when the buoyancy flux goes to zero, can be related to the peak of the cospectra of the buoyancy flux. This new relationship can be used to provide a measure of the smallest turbulent scale in cases where the buoyancy flux never goes to zero, i.e. a growing turbulent stratified shear flow. Finally, the one-dimensional energy transfer term computed from the bispectra shows evidence of a reverse energy cascade from the small scales to the large scales far from the grid where buoyancy forces dominate inertial forces. The observed reverse energy transfer could be produced by the development of quasi-two-dimensional eddies as the original three-dimensional turbulence collapses.

1. Introduction

Recent observations in the atmosphere and the oceans shows large isolated two-dimensional vortex-like structures. Such eddies can result from the Coriolis effects as well as the large ratio between horizontal and vertical dimensions of the atmosphere or the oceans. Two-dimensional eddies can also be obtained in laboratory geophysical flows such as very stably stratified flows (Lin & Pao 1979), fast rotating flows (Hopfinger, Griffiths & Mory 1983) or magnetohydrodynamic (MHD) flows (Sommeria & Moreau 1982). Some of the large-scale coherent structures such as those formed in a mixing layer (Brownand & Winant 1973; Koop & Browand 1979) also appear to be two-dimensional. Several questions arise: are such eddies truly two-dimensional, and how is their evolution coupled to smaller three-dimensional

† Present address: Data Ready, Suite 150, 4647 T Highway 280 East, Birmingham, AL 35242, USA.

turbulent scales? It is also likely that in most geophysical flows there will be an evolution from a three-dimensional turbulent flow with or without waves (internal or Rossby waves for example) to a quasi-two-dimensional flow as growing turbulent scales become limited in size by external constraints (physical dimension, buoyancy effects, electromagnetic forces, Coriolis forces or any combination of these). Several theories such as the test field model (TFM, Kraichnan 1971) and the eddy-damped quasi-normal Markovian theory (EDQNM, Orszag 1974) as well as recent high-resolution direct simulations (Herring *et al.* 1974; Herring & McWilliams 1985) provide a framework for a purely two-dimensional turbulence and its spectral properties. Both TFM and EDQNM show that in the inertial–diffusive region, the concept of enstrophy cascade produces an energy spectrum falling off like k^{-3} while the corresponding scalar spectrum is k^{-1}. Both of these spectral shapes have been observed in MHD turbulence (Sommeria 1983) and fast rotating flows (Hopfinger *et al.* 1983). Gower, Denman & Holyer (1980) reported a k^{-3} spectra from surface phytoplankton concentration measurements in the ocean. These observations and temperature (scalar) measurements in the ocean seem to indicate that, in the enstrophy cascade region, the energy spectra would have a steeper slope (k^{-4} to k^{-5}) than the k^{-3} slope predicted by the theories. Herring & McWilliams (1985) numerical experiments showed that in a spin-down problem (no energy input at the large scales) the two-dimensional flow would evolve into a small number of independent vortices. This spatial intermittency is characterized by a k^{-4} slope in the entrophy cascade region of the energy spectrum.

Before one tries to compare laboratory experiments to various theories, it is necessary to first determine at what point in the evolution of the flow these theories might apply. Let us consider the case of strongly stratified turbulent flows, which is the scope of this paper. Gibson (1980), Stillinger *et al.* (1983*a*) and Stillinger, Helland & Van Atta (1983*b*) (the latter two are hereinafter referred to as SHV) independently derived lengthscale arguments to characterize the state of fluid motion, i.e. isotropic turbulence or fossil turbulence and internal waves. Many of the previous laboratory experiments in stably stratified flows did not include simultaneous single-point measurements of the vertical velocity and density (Lin & Veenhuizen 1975; Dickey & Mellor 1980; Lange 1982; Britter *et al.* 1983). Only recently, SHV and Itsweire, Helland & Van Atta (1986, hereinafter referred to as IHV) made such measurements and estimated the buoyancy flux $(g/\bar{\rho})\overline{\rho w}$. Both SHV and IHV used, for the first time, the buoyancy flux going to zero as a criterion for the extinction of overturning turbulence. SHV followed the idea advanced by Stewart (1969) that linear internal waves have their vertical velocity w and density fluctuation ρ in quadrature and therefore do not contribute to the buoyancy flux. Consequently, the buoyancy flux is assumed to come only from turbulent contributions and when turbulent events are suppressed by buoyancy, $(g/\bar{\rho})\overline{\rho w}$ goes to zero. This criterion is an approximation for the extinction of turbulence (in the three-dimensional, isotropic Kolmogorovian sense) since nonlinear internal waves, fossil vorticity turbulence (Gibson 1980) and large-scale restratification can produce some vertical mixing.

The prime objectives of this study are to investigate more fully the spectral characteristics of the buoyancy flux and to examine energy transfer properties of the downstream velocity component. Some preliminary results for the buoyancy flux spectra were presented in previous papers (Van Atta, Helland & Itsweire 1984; IHV). Energy transfer is estimated by using third-order bispectral techniques at various downstream distances from a turbulence generating grid; of special interest is the possibility of detecting by statistical methods a reversal in the *direction* of

spectral energy transfer after the collapse of three-dimensional turbulence into a state of quasi-two-dimensional motions (two-dimensional turbulence). The experience acquired from a number of earlier experiments (e.g. SHV and IHV) provided critical information used to guide the choice of stratification, grid design, measurement locations and record duration to best achieve these objectives.

A number of investigators have offered estimates of the buoyancy flux in terms of the mixing efficiency of the flow using various eddy diffusivity models (Weinstock 1978; Osborn 1980; Pearson, Puttock & Hunt 1983). Rohr, Itsweire & Van Atta (1984) calculated the mixing efficiency of the flow from direct measurements of the buoyancy flux and the dissipation rate ϵ. They found that the mixing efficiency depended on the ratio between the buoyancy and inertial forces. It is very interesting to look at the wavenumber distribution of the buoyancy flux in order to assess how much mixing is due to turbulence, and how much is due to waves and fossil vorticity turbulence. Itsweire & Helland (1985) reported some preliminary results on the cospectra of ρ and w. Their results from the data of SHV show that up to 10% of the mixing can come from non-turbulent scales.

Third-order spectra, known as bispectra can be useful to examine nonlinear interactions in turbulent flows. Lii, Rosenblatt & Van Atta (1976) and Helland, Lii & Rosenblatt (1979) showed that accurate bispectral estimates could provide insight in the analysis of spectral energy transfer in three-dimensional turbulence. Lii *et al.* (1976) concluded that both the spectral energy transfer due to triadic interactions and the rate of vorticity production were non-local, meaning that, on the average, vortices of broadly different scales interacted. Other approaches (Wilson 1974; Van Atta 1979) combined bispectral estimates to compute the local one-dimensional energy transfer due to wavenumber interactions. These calculations showed that, in three-dimensional turbulence, energy cascades from the large to small scales as could be expected. In a stratified environment, if the turbulence collapses into quasi-two-dimensional turbulence, the energy cascade could be reversed as predicted by two-dimensional turbulence simulations (Herring *et al.* 1974). However, recent direct numerical simulations of stratified turbulence (Métais & Herring 1989) are inconclusive in this respect.

Section 2 describes the experimental conditions for the new data sets and the UCSD water channel facility. A brief view of the stratified turbulence lengthscale model is presented in §3. The theoretical derivations of the one-dimensional energy transfer from the bispectrum are shown in §4. Section 5 compares different methods for indirectly estimating the buoyancy flux with direct measurements and examines the spectral distribution of the buoyancy flux cospectra. Section 6 shows the evolution of the shapes of the velocity and density power spectra with increasing buoyancy effects and compares them with theoretical predictions for two-dimensional turbulence. Third-order spectra or bispectra are presented in §7. Finally, one-dimensional energy transfer estimates calculated from the bispectra and their implications on the evolution of the turbulence in stratified flows are discussed in §8.

2. Experiments

The present experiments were conducted in the ten-layer closed-loop salt-stratified water channel in the Department of Applied Mechanics and Engineering Sciences at the University of California, San Diego. The general layout of the facility and the instrumentation has been described in great detail by Stillinger *et al.* (1983*a*). Only

Experiment	Grid type	M (cm)	Number of records	Record length (s)
R53	Biplane grid	1.905	24	8
R64	Vertical rods	3.81	50	16
R65	Vertical rods	3.81	50	16

TABLE 1. Experimental parameters for the two stratified experiments (R53 and R64) and the unstratified experiment (R65)

modifications in the tunnel and changes in the data acquisition parameters will be discussed in this paper.

In addition to the data of SHV and IHV three new experiments, R53, R64 and R65, will be examined. We used the results of SHV and IHV to limit our measurements to critical stations downstream from the grid, i.e. before the onset of buoyancy effects, in the buoyancy-dominated region and after the extinction of three-dimensional overturning events.

The number of data records at each measurement location was increased from 6 to 50 in order to attain a good resolution of the cospectra and bispectra. In experiments R64 and R65 the record length was doubled to 16 s from the earlier value of 8 s. Also the small mesh ($M = 1.905$ cm) grid of R23, R52 and R53 was replaced by an array of vertical rods of diameter $d = 0.636$ cm and horizontal spacing $M = 3.81$ cm. The horizontal rods present in R36 and R37 were removed in order to further reduce the generation of an internal wave field and increase the initial ratio between the root-mean-square horizontal velocity u' and the root-mean-square vertical velocity w'. By these means, we hoped to promote the generation of a quasi-two-dimensional turbulence closer to the ideal limit of two-dimensional turbulence. Only these last two experiments (R64 and R65) were used to compute the bispectra and the deduced one-dimensional energy transfer terms. The experimental parameters of the various experiments are summarized in table 1.

The instrumentation and experimental arrangement are identical to previous work in the UCSD water channel (SHV; Rohr *et al.* 1984; and IHV). The calibration procedures for the $\times$-film sensor and the 4-wire microscale conductivity instrument (MSCI, see Head 1983) are described in detail in Stillinger *et al.* (1983*a*). The water channel was controlled by the laboratory LSI 11/23 microcomputer. This computer equipped with a 14-bit A/D converter and ten channels of sample-and-hold circuitry was also used to digitize the data and perform all the calibration computations and data analysis.

3. Lengthscale models of stratified turbulence

The dynamics of stably stratified turbulent flows are governed by the relative ratios among three different forces, i.e. buoyancy, inertial and viscous forces. Buoyancy forces will create an upper ceiling for the growth of turbulent eddies, while viscous forces will limit the size of the smallest overturning eddies. Gibson (1980, 1986) predicted the range of possible overturning turbulent scales (in the three-dimensional, Kolmogorovian sense) to be

$$1.2L_{\mathrm{O}} \geqslant \lambda \geqslant 15L_{\mathrm{K}}, \tag{1}$$

where $L_{\mathrm{O}} = (\epsilon/N^3)^{\frac{1}{2}}$ is the Ozmidov scale (Dougherty 1961; Ozmidov 1965) representing the action of buoyancy forces, $L_{\mathrm{K}} = (\nu^3/\epsilon)^{\frac{1}{4}}$ the Kolmogorov scale

indicating the viscous effects, and λ a turbulent wavelength. Independently, Stillinger (1981) and SHV found experimentally that the range of possible turbulent scales for the grid-generated turbulence in their stratified water channel was:

$$1.4L_O \geqslant l \geqslant 15.5L_K. \tag{2}$$

They defined the largest turbulent scale (in a statistical sense) of their flow as twice the turbulent scale L_t first introduced by Ellison (1957):

$$L_t = \frac{-\rho'}{\partial\bar{\rho}/\partial z} \tag{3}$$

where ρ' is the root-mean-square (r.m.s.) density fluctuation. SHV used simple solid-body rotation to model the largest turbulent eddy in terms of L_t. Such a representation is physically oversimplified but seems to give a good estimate of the largest turbulent eddy size in their experiments (Itsweire 1984).

The result (2) was recently refined by IHV who noted some dependence of the proportionality factors on the grid mesh size. They found that the onset of buoyancy effects (beginning of fossilization) occur when

$$L_t = 0.85L_O \tag{4}$$

and that the turbulence becomes extinct (complete fossilization) when

$$L_O = 7.6L_K \quad \text{for} \quad M = 1.905 \text{ cm} \tag{5a}$$

or

$$L_O = 9.9L_K \quad \text{for} \quad M = 3.81 \text{ cm}. \tag{5b}$$

The uncertainty in the ratios between the various lengthscales is estimated to be around 6%.

The onset of buoyancy effects (or beginning of fossilization, Gibson 1980) is taken to be at the x/M station in the tunnel where the evolution of the r.m.s. density fluctuation ρ' departs from the passive-scalar growth law of Montgomery (1974), because buoyancy is expected to limit the growth of turbulent scales.

For the extinction of all overturning turbulent motions (or complete fossilization, Gibson 1980), SHV followed Stewart's (1969) ideas that for a linear internal wave field the vertical velocity and the density fluctuation are 90° out of phase, and thus the buoyancy flux $(g/\bar{\rho})\overline{\rho w}$ is zero and no vertical mixing takes place. This criterion $\overline{\rho w} \approx 0$ is rigorously true only for linear waves and may on average be valid for weakly nonlinear waves. At the x/M station where $\overline{\rho w} \approx 0$, SHV and IHV determined the ratio between the Kolmogorov scale L_K and the smallest overturning scale of the flow (see (5)).

4. Theoretical derivations for the energy transfer calculations

Let us consider the Navier–Stokes equation for the longitudinal velocity component u:

$$\frac{\partial u}{\partial t} + u\frac{\partial u}{\partial x} + \ldots = -\frac{1}{\rho}\frac{\partial p}{\partial x} + \nu\nabla^2 u. \tag{6}$$

Only the first two terms are considered through their complex Fourier series. The complex Fourier representation of $u(x,t)$, with respect to the longitudinal direction x, is defined as

$$u(x,t) = \Delta k \sum_k F_u(k,t)\, e^{ikx}, \quad k = (p-1)\,\Delta k, \quad p = 1, \ldots, (\tfrac{1}{2}n+1), \tag{7}$$

where time t is included temporarily in $F_u(k,t)$ to indicate that the complex Fourier coefficients are functions of only time and not space. The record length is taken to be $n\Delta x = 1/\Delta k$. After substitution of the Fourier series for $u(x,t)$, (6) becomes

$$\Delta k \frac{\partial}{\partial t} \sum_k F_u(k)\, e^{ikx} + (\Delta k)^2 \sum_m F_u(m)\, e^{imx} \frac{\partial}{\partial x} \sum_k F_u(k)\, e^{ikx} + \ldots, \tag{8}$$

where separate wavenumbers k and m have been used for the two velocities in the second term. Since we are ultimately seeking the interaction among different longitudinal wavenumbers, we multiply (8) by the Fourier component $F_u(l)\, e^{ilx}$, where l is a third wavenumber:

$$\Delta k F_u(l)\, e^{ilx} \frac{\partial}{\partial t} \sum_k F_u(k)\, e^{ikx} + (\Delta k)^2 F_u(l)\, e^{ilx} \sum_m F_u(m)\, e^{imx} \frac{\partial}{\partial x} \sum_k F_u(k)\, e^{ikx} + \ldots. \tag{9}$$

The derivative $\partial/\partial x$ of the second term can be expressed as

$$\frac{\partial}{\partial x} \sum_k F_u(k)\, e^{ikx} = \sum_k ikF_u(k)\, e^{ikx}. \tag{10}$$

Then, after collecting the exponentials inside the summations, (9) becomes

$$\Delta k F_u(l) \frac{\partial}{\partial t} \sum_k F_u(k)\, e^{i(l+k)x} + (\Delta k)^2 \sum_m \sum_k ikF_u(l)\, F_u(m)\, F_u(k)\, e^{i(l+m+k)x} + \ldots. \tag{11}$$

Taking the average over the record length $n\Delta x$, dividing by 2π and using the orthogonality condition

$$\sum_0^{n\Delta x} e^{i(l+k)x} = 2\pi n \delta_{l+k} \tag{12}$$

(11) becomes

$$\Delta k F_u(l) \frac{\partial}{\partial t} \sum_k F_u(k)\, \delta_{l+k} + (\Delta k)^2 \sum_m \sum_k ikF_u(l)\, F_u(m)\, F_u(k)\, \delta_{l+m+k} + \ldots. \tag{13}$$

The orthogonality condition δ_{l+k} requires that $l+k=0$ for the first term to be non-zero, and δ_{l+m+k} requires that $l+m+k=0$ for the second term to be non-zero. Using the definitions of the one-dimensional spectrum

$$\begin{aligned} E_{u,u}(l) &\equiv \Delta k F_u(l)\, F_u(k)\, \delta_{l+k}, \quad l+k=0 \\ &= \Delta k F_u(l)\, F_u^*(l) = \Delta k |F_u(l)|^2 \end{aligned} \tag{14}$$

and the one-dimensional bispectrum of the longitudinal velocity component

$$B_{u,u,u}(l,m,k) \equiv \Delta k F_u(l)\, F_u(m)\, F_u(k), \quad l+m+k=0, \tag{15}$$

and applying the Hermitian symmetry $F_u(-l) = F_u^*(l)$, where F_u^* is the complex conjugate of F_u, (13) becomes

$$\frac{\partial}{\partial t}[\tfrac{1}{2}E_{u,u}(l)] + \Delta k \sum_k \sum_m ikB_{u,u,u}(l,m,k) + \ldots, \quad l+m+k=0. \tag{16}$$

If the summations over wavenumbers k and m are performed, we are left with an equation in l that is a one-dimensional version of the usual three-dimensional energy transfer equation. We are more interested in the interactions between wavenumbers l and k. Choosing these two wavenumbers determines the value of the third wavenumber $m = -l-k$. This approach requires that, for each pair (l,k), we sum

over all possible values of wavenumber m as required by the inner summation in (16). We define the quantity $S(k;l)$ by

$$S(k;l) = \Delta k \,\mathrm{Re}\,[\mathrm{i}k \sum_{m=-l-k} F_u(l)\,F_u(m)\,F_u(k)] = \mathrm{Re}\,[\mathrm{i}k \sum_{m=-l-k} B_{u,u,u}(l,m,\ k)]$$

$$= -k \sum_{m=-l-k} \mathrm{Im}\,[B_{u,u,u}(l,m,k)]. \quad (17)$$

The physical meaning of the $S(k;l)$-spectrum is indicated by the Navier–Stokes equation to be the net transfer of energy between wavenumber l and wavenumber k through triadic interactions. Equation (16) can be rewritten as

$$\frac{\partial}{\partial t}[\tfrac{1}{2}E_{u,u}(l)] = -\Delta k \sum_k S(k;l) + \ldots. \quad (18)$$

The first term of the right-hand side of (18) can be written in terms of a one-dimensional net transfer term $T_u(l)$ for the longitudinal velocity component u:

$$T_u(l) = \Delta k \sum_k S(k;l). \quad (19)$$

By examining the implications of the orthogonality constraint $l+m+k=0$, given selected values of l and k, we can determine the possible values of wavenumber m. Recall that these wavenumbers are purely one-dimensional, so that there are no vector triangles to consider as would be the case for the full three-dimensional transfer term. Since l, m, k can be of either sign, the summation over m can be at most over one term unless we ignore the signs in the summation. This is the right approach to consider if one only needs the wavenumber magnitudes, not their directions. Thus the summation will reduce to two terms for any choice of l and k where $l > 0$. The analysis can be limited to the right half-plane ($l > 0$) because the Hermitian symmetry property $B(-l,-m,-k) = B^*(l,m,k)$ of the bispectrum of a real time series implies that the left-half-plane contribution equals that of the right half-plane.

If we now redefine the three wavenumber symbols as positive scalars without their sign, the orthogonality condition over the right half-(l,m)-plane can then be expressed as

$$l \pm m \pm k = 0. \quad (20)$$

The sum $l+m+k$ is >0 since all three wavenumbers are positive by our new restrictions on the definitions of l, m, k. By considering all possible sign combinations of m and k with $l > 0$, we can construct only three types of wavenumber interactions (combinations of l, m, k which sum to 0).

Type 1: $l-m+k=0$

This interaction corresponds to the bispectrum $B_{u,u,u}(l,-m,k)$ with $m = l+k$, $k > 0$ or, after expressing m in terms of l and k, $B_{u,u,u}(l,-(l+k),k)$. Recall that all wavenumbers are now positive and that the signs are carried explicitly everywhere.

Type 2: $l-m-k=0$

This interaction corresponds to the bispectrum $B_{u,u,u}(l,-m,-k)$ with $m = l-k$, $k < l$ or, after expressing m in terms of l and k, $B_{u,u,u}(l,-(l-k),k)$. The restriction that $k < l$ is required to keep $m > 0$.

Type 3: $l+m-k=0$

This interaction corresponds to the bispectrum $B_{u,u,u}(l,m,-k)$ with $m = k-l$, $k > l$ or, after expressing m in terms of l and k, $B_{u,u,u}(l,k-l,k)$.

The three types of interaction are numbered identically to the terms that Wilson (1974) derived independently. The three interactions can be combined into one expression for $S(k;l)$:

$$S(k;l) = \mathrm{Re}\,[\mathrm{i}kB_{u,u,u}(l,-(l+k),k)]\begin{cases}-\mathrm{Re}\,[\mathrm{i}kB_{u,u,u}(l,-(l-k),-k)], & k<l\\ -\mathrm{Re}\,[\mathrm{i}kB_{u,u,u}(l,k-l,-k)], & k>l,\end{cases} \tag{21}$$

where l, m, k are all positive scalars. The sign of the k-factor in front of each bispectrum follows the sign of its third wavenumber because of the derivative $\partial/\partial x$. We can rewrite (21) in terms of the imaginary part of the bispectrum:

$$S(k;l) = -k\,\mathrm{Im}\,[B_{u,u,u}(l,-(l+k),k)]\begin{cases}+k\,\mathrm{Im}\,[B_{u,u,u}(l,-(l-k),-k)], & k<l\\ +k\,\mathrm{Im}\,[B_{u,u,u}(l,+(k-l),-k)], & k>l.\end{cases} \tag{22}$$

By using the symmetry properties of the bispectrum (Lii & Helland 1981), the bispectrum in the lower-right quadrant (terms 1 and 2) can be mapped into the bispectrum defined in the upper-right quadrant. Details of the transformations for the present case are shown in Appendix A. After the transformations, (22) becomes

$$S(k;l) = -k\,\mathrm{Im}\,[B_{u,u,u}(l,k)]\begin{cases}-k\,\mathrm{Im}\,[B_{u,u,u}(k,l-k)\}, & k<l\\ +k\,\mathrm{Im}\,[B_{u,u,u}(l,k-l)], & k>l,\end{cases} \tag{23}$$

where the explicit third wavenumber has been dropped. This expression for $S(k;l)$ is different from the one in Helland, Itsweire & Lii (1985), which is incorrect.

Finally if we were to sum $S(k;l)$ of (17) over all positive k and l we obtain

$$\overline{uu\frac{\partial u}{\partial x}} = 2(\Delta k)^2 \sum_l \sum_k S(k,l) = 2\Delta k \sum_l T_u(l), \tag{24}$$

where the factor of 2 accounts for the contribution from the left half-plane.

5. Estimates and spectral distribution of the buoyancy flux

5.1. *Estimates of the buoyancy flux*

Measurements of the vertical mass flux or buoyancy flux in geophysical flows are hard to achieve because they require simultaneous single-point measurements of the vertical velocity and the conductivity or temperature fluctuations at scales on the order of several millimetres. Consequently several methods referred to as dissipation techniques requiring various assumptions have been developed to indirectly estimate the buoyancy flux for given atmospheric and oceanic situations. The common assumption is that the flow is approximately in steady state and that the kinetic energy dissipation rate ϵ can be obtained from small-scale velocity shear measurements. Osborn (1980) made some additional assumptions about the energy partitioning between potential kinetic energies, i.e. at equilibrium the flux Richardson number R_f reaches a critical value of 0.15 (Ellison 1957). Then, Osborn (1980) estimates the buoyancy flux as

$$(g/\bar{\rho})\overline{\rho w} \leqslant 0.20\epsilon. \tag{25}$$

The value 0.20 proposed by Osborn (1980) agrees well with recent oceanographic estimates by Oakey (1982) and Gregg *et al.* (1986) and laboratory experiments where the Richardson number Ri is near a critical value of 0.25 (Rohr & Van Atta 1987).

Eddy diffusivity models have been used by Weinstock (1978) and Pearson *et al.*

(1983) to estimate the buoyancy flux. Weinstock (1978) analytically derived the vertical turbulent diffusion coefficient K_z for a high-Reynolds-number stably stratified turbulent flow, i.e. with an inertial subrange. The derived value of K_z as a function of the kinetic energy dissipation rate ϵ and the Brunt–Väisälä frequency N is

$$K_z \approx 0.81\,(\epsilon/N^2). \tag{26}$$

Equation (26) can be rewritten in terms of the buoyancy flux as

$$(g/\bar{\rho})\,\overline{\rho w} \approx 0.81\epsilon. \tag{27}$$

Weinstock (1978) noted that his derivation for the vertical diffusion coefficient K_z is 'quite general for stable stratification because it does not depend on the mechanism of turbulent production nor an assumed value of the Richardson number'. In fact the only restriction in Weinstock's derivation is the assumption of the existence of an inertial subrange and that only scales in this subrange contribute to the vertical turbulent diffusion. Consequently, this derivation may not be valid for low-Reynolds-number flows such as the ones obtained in laboratory experiments.

Comparisons between the buoyancy flux directly measured by SHV and IHV in a stratified water channel at small Reynolds numbers and (27) applied to the same data show that Weinstock's expression for the vertical turbulent diffusivity overestimates the buoyancy flux by a factor of 4–5. The discrepancy between the constant in (25) and (27) has yet to be explained.

Pearson *et al.* (1983) developed a statistical model for the particle displacement and vertical diffusion in a stably stratified turbulent flow. They assumed the turbulence to be statistically stationary and homogeneous, conditions similar to our laboratory experiments, and concluded that for stable flows the buoyancy flux could be approximated as

$$(g/\bar{\rho})\,\overline{\rho w} = \gamma w'^2 N, \tag{28}$$

where γ is a measurable parameter. Pearson *et al.* (1983) do not say how to determine γ but report values ranging from 0.1 and 0.4 for several measurements in the atmospheric surface layer. It appears that the parameter γ is a function of the stratification, or equivalently a function of the ratio between buoyancy and inertial forces. Therefore (28) can only provide an order of magnitude estimate for the buoyancy flux. If one assumes that the buoyancy scale $L_b = w'/N$ is equivalent to the Ozmidov scale (see IHV) then (28) can be rewritten as

$$(g/\bar{\rho})\,\overline{\rho w} = \gamma\epsilon. \tag{29}$$

Therefore the parameter γ can be thought of as being proportional to the mixing efficiency. Rohr *et al.* (1984) showed that for a decaying stratified turbulent flow with a uniform mean velocity the mixing efficiency of the flow was a strong function of the ratio between inertial and buoyancy forces. The measured values of the mixing efficiency varied between 0.1 and 0.2 for a buoyancy-influenced turbulent flow. This result implies that Osborn's (1980) choice of an average mixing efficiency (or equivalently γ) of 15% would provide a reasonable estimate of the buoyancy flux in most cases.

Figure 1 shows the correlation coefficient (normalized buoyancy flux) versus normalized downstream distance from the grid for the two stratifications of experiment R53. The maximum of about 0.4 in this correlation coefficient occurs shortly after the onset of buoyancy effects as noted previously by SHV and IHV. At that point the vertical eddy diffusivity is $K_z \approx 0.18\epsilon$. Direct numerical simulations

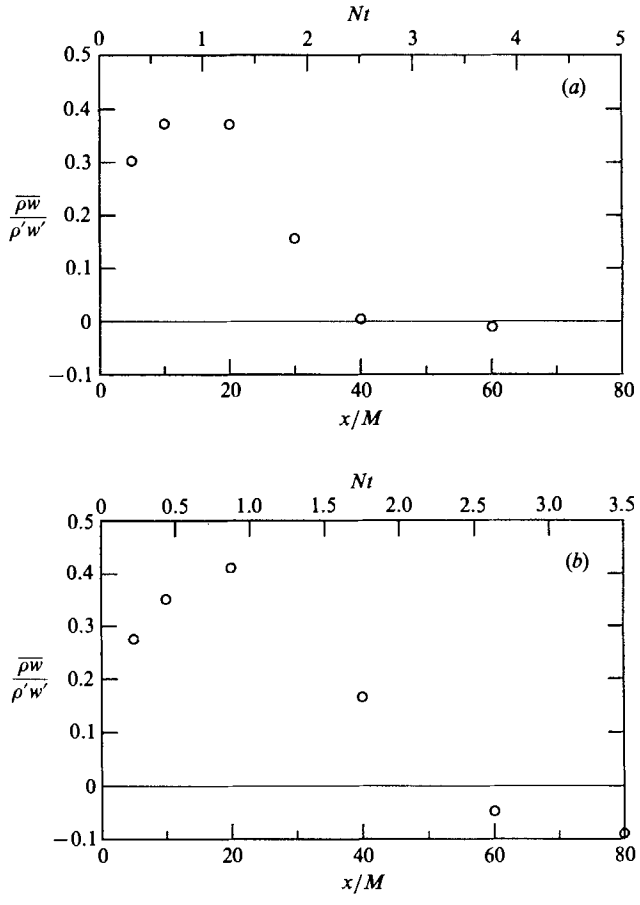

FIGURE 1. Non-dimensional buoyancy flux $\overline{\rho w}/\rho' w'$ *vs.* downstream distance from the grid x/M for R53; (*a*) $N = 0.91$ s^{-1}; (*b*) $N = 0.65$ s^{-1}.

(Riley, Metcalfe & Weissman 1981; Métais 1985) imply that, after the first zero crossing, the buoyancy flux oscillates between negative and positive values with a period equal to the buoyancy period. Larger x/M-values would be needed to resolve and characterize this oscillatory behaviour of the buoyancy flux around zero after the first zero crossing. The maximal value reached by the correlation coefficient $\overline{\rho w}/\rho' w'$ seems to be a function of the Prandtl or Schmidt number (depending on the stratification agent). Experiments in wind tunnels where differential heating produces the density gradient (Sirivat & Warhaft 1983; Lienhard 1988) show a maximum correlation value of 0.70.

5.2. *Spectral distribution of the buoyancy flux*

Both dissipation-rate and eddy-diffusivity models for the buoyancy flux can, at best, estimate its order of magnitude but cannot tell us which scales are contributing to the vertical mixing. It has been suggested (Stewart 1969) that only the small turbulent scales produce any vertical mixing ($(g/\bar{\rho})\overline{\rho w} > 0$) and that some restratification ($(g/\bar{\rho})\overline{\rho w} < 0$) could occur at larger scales.

Figure 2 shows a comparison of the buoyancy flux cospectrum with the energy spectra and the dissipation spectra for two stations of figure 1(*a*) ($x/M = 5$ and 20,

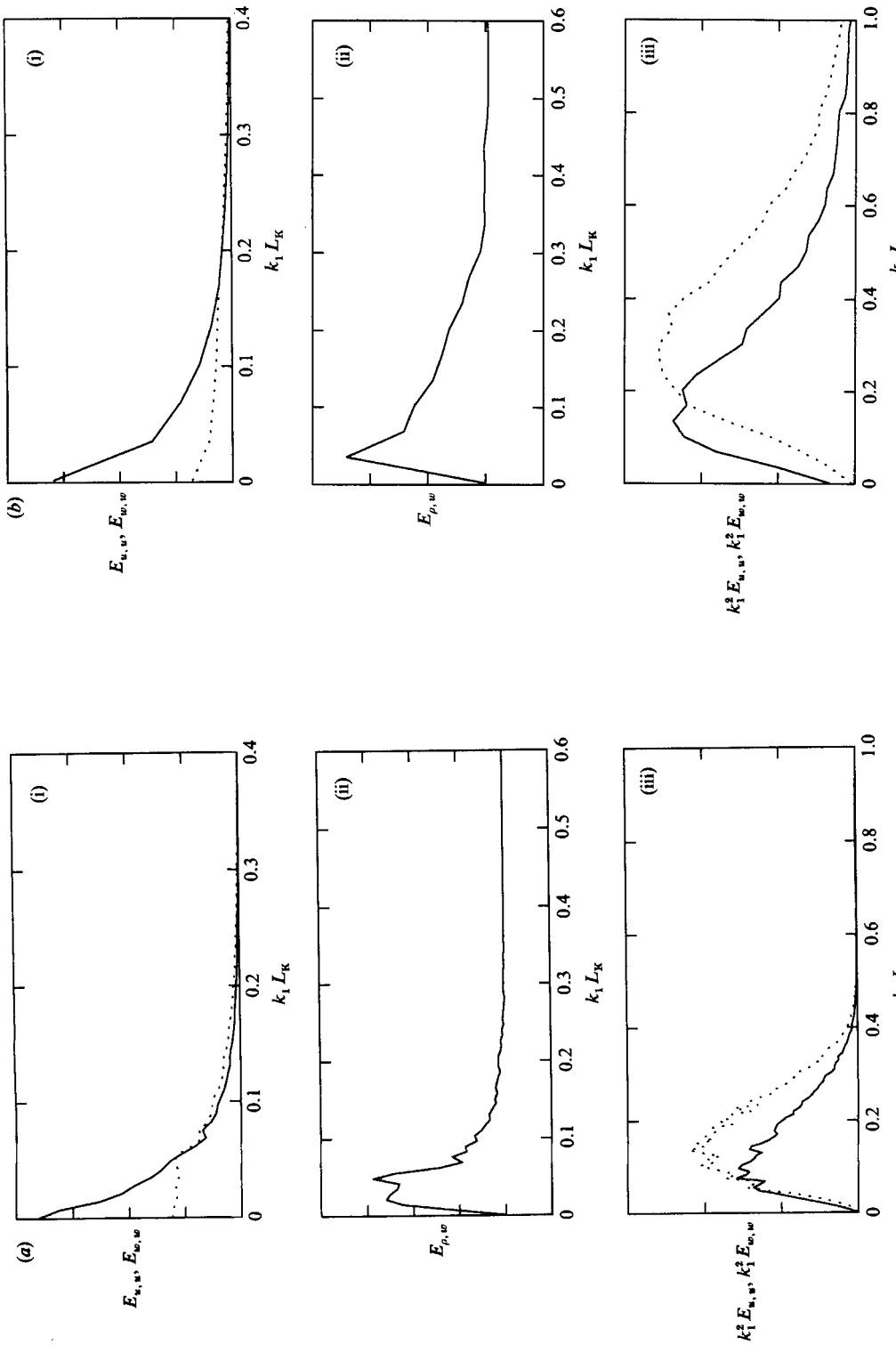

FIGURE 2. Comparison between the velocity power spectra, buoyancy flux cospectrum and dissipation spectra for two stations of R53, $N = 0.91\ \mathrm{s}^{-1}$; (*a*) $x/M = 5$; (*b*) $x/M = 20$. All spectra are one-dimensional spectra and the longitudinal wavenumber k_1 is normalized by the Kolmogorov scale L_K. The vertical axes are in arbitrary units. In (i) and (iii) the solid line refers to the longitudinal velocity component u and the dotted line to the vertical velocity component w.

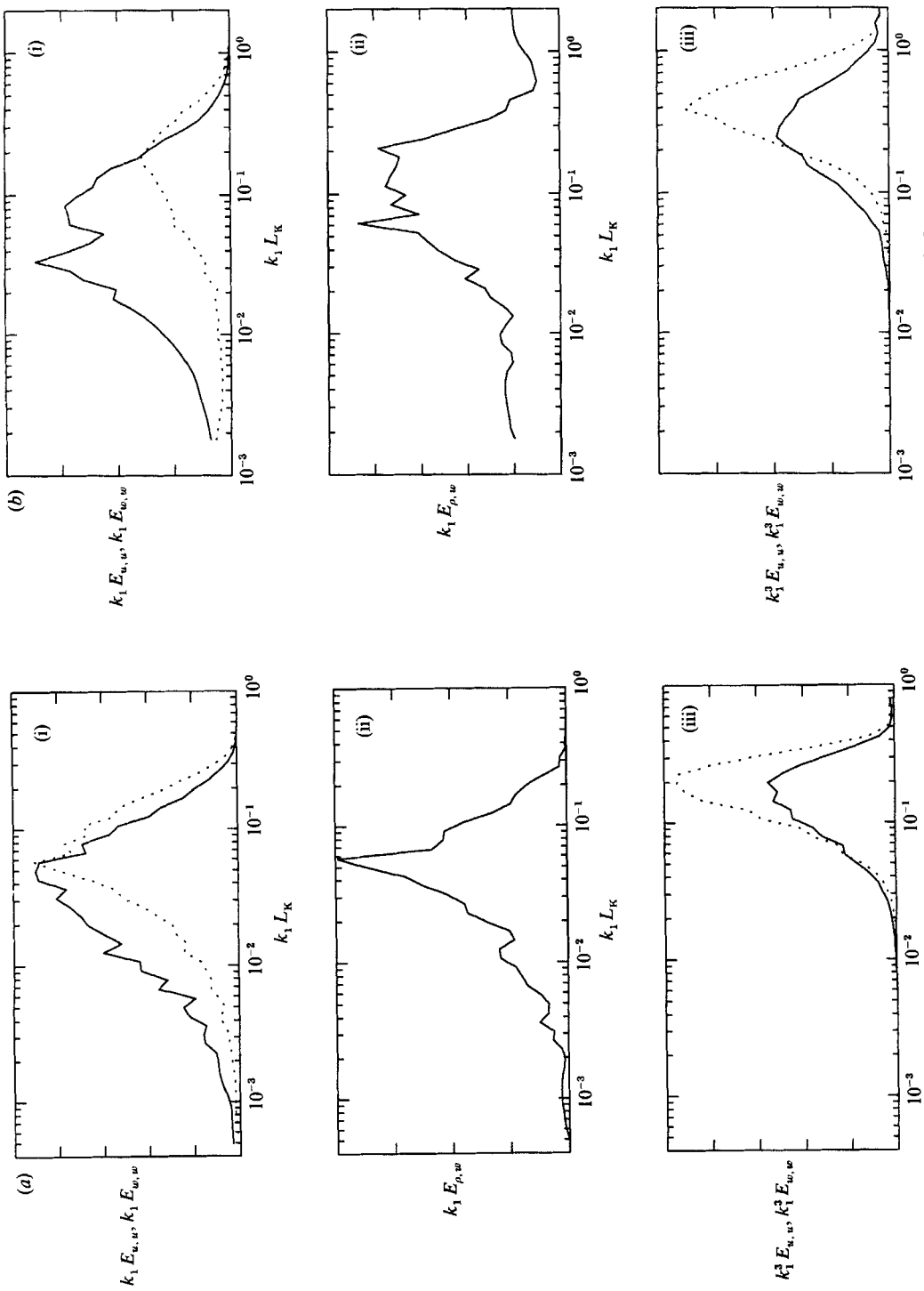

FIGURE 3. Comparison between the velocity power spectra, buoyancy flux and dissipation spectra for the data of figure 2 in variance-preserving coordinates. Curves are labelled as in figure 2.

respectively of R53). All spectra are one-dimensional as defined in §4. The original measured frequency dependence (f) has been transformed into a longitudinal wavenumber dependence ($k_1 = 2\pi f/\bar{U}$) with Taylor's assumption of a frozen turbulent field:

$$E_{x,y}(k_1) = \frac{\bar{U}}{2\pi} E_{x,y}(f), \tag{30}$$

where $\bar{U}$ is the mean speed of the flow.

Near the biplane grid (R52 and R53), the turbulence is nearly isotropic and buoyancy effects are dynamically unimportant (see SHV and IHV). SHV's comparisons between the vertical velocity spectrum $E_{w,w}$ and the corresponding spectra computed from the longitudinal velocity spectrum $E_{u,u}$ (see (31) in §6) showed that the anisotropy is confined to low frequencies (large scales). The initial ratio between the turbulent intensities $u'/w' \approx 1.15$ is comparable with wind tunnel measurements. The observed degree of anisotropy of the turbulence field in the UCSD water channel is acceptable considering the limitations of the facility, which does not include any contraction section similar to the one used in wind tunnels (Comte-Bellot & Corrsin 1966). The dissipation spectrum of the longitudinal velocity $k_1^2 E_{u,u}(k_1)$, shown in figure 2(iii), peak at about 10 Kolmogorov scales L_K, in good agreement with atmospheric turbulence measurements and moderate to high Reynolds number laboratory experiments (Yeh & Van Atta 1973; Champagne 1978). For both x/M locations shown in figure 2, the lengthscales containing the turbulent kinetic energy appear to generate most of the buoyancy flux. In addition, lengthscales below the dissipation peak, which is usually taken to be the viscous cutoff wavenumber, contribute as much as 10% of the buoyancy flux. The relative contribution of specific wavenumber bands is better visualized when the velocity and dissipation spectra and the buoyancy flux cospectrum of figure 2 are plotted in variance-preserving coordinates, figure 3, with a logarithmic wavenumber or frequency axis. The variance-preserving coordinate system is the best coordinate system to compare the range of scales or frequencies contributing to different spectra as shown in figure 3. The one drawback of this coordinate system is that it shifts the wavenumber of the spectrum peak to higher values. The amount of this shift is highly dependent on the slope of the spectrum near the peak wavenumber. For the data of figures 2 and 3, the peak of $k_1 E_{\rho,w}$ is located at approximately $18L_K$, compared with the peak of $E_{\rho,w}$ occurring at $30L_K$.

Figure 4 shows the buoyancy flux spectral distribution $k_1 E_{\rho,w}$ in variance-preserving coordinates which emphasize the midwavenumbers which contribute the most to the flux. A similar behaviour in the buoyancy flux spectrum was observed for the data sets of SHV and IHV. The cospectra $E_{u,w}$ and $E_{\rho,u}$ corresponding to the two decays of figure 1 are essentially zero except near the grid ($x/M \leqslant 10$), where the distinct wakes of the grid rods may still be significant.

Two important results can be obtained by comparing the values of the buoyancy flux $(g/\bar{\rho})\overline{\rho w}$ of figure 1 and their spectral contents shown in figure 4. The first result, that was alluded to by IHV, concerns the verification of SHV's assumption that a zero buoyancy flux $(g/\bar{\rho})\overline{\rho w}$ means that no vertical mixing takes place. It is remarkable and satisfying to find that, when the buoyancy flux goes to zero, its spectrum becomes identically zero across all wavenumbers. This is an important finding, since $(g/\bar{\rho})\overline{\rho w} = 0$ only implies that the sum of the cospectrum estimates over all wavenumbers will be zero. This result supports SHV's and IHV's earlier assumption that a buoyancy flux $(g/\bar{\rho})\overline{\rho w}$ going to zero meant the suppression of turbulent mixing at all scales. It should be noted that this result is not universal, but

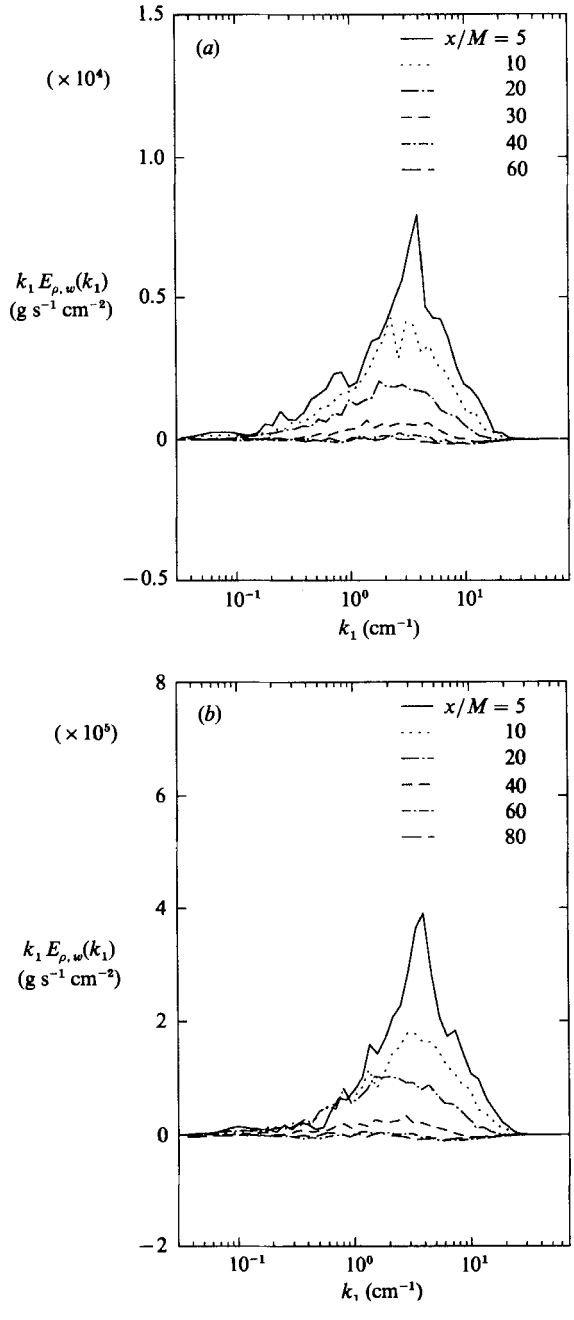

FIGURE 4. Spectral content of the buoyancy fluxes shown in figure 1. All the data are from the two decays of R53; (*a*) $N = 0.91$ s^{-1}; (*b*) $N = 0.65$ s^{-1}.

appears to depend on the value of the Prandtl or Schmidt number. Recent measurements in stratified wind tunnel (Lienhard 1988) show that, in a turbulent flow with low Prandtl number ($Pr = 0.7$), a counter-gradient transport occurs at the largest scales, suggesting partial restratification, while active vertical mixing continues at the small scales ($(g/\bar{\rho})\overline{\rho w} > 0$). Additional experiments with different

Experiment	M (cm)	N (s^{-1})	L_{peak}/L_K	L_{min}/L_K
R37	3.810	0.93	19.0	3.50
(IHV)	3.810	0.74	18.2	3.30
R52	1.905	0.93	18.0	2.50
(IHV)	1.905	0.73	19.0	2.45
	1.905	0.50	20.0	2.45
R53	1.905	0.91	18.0	2.36
	1.905	0.65	16.5	2.25
R64	3.810	0.90	18.9	3.40
	3.810	0.64	19.1	3.20

TABLE 2. Relationship between the Kolmogorov scale L_K, the scale at which $k_1 E(\rho, w)$ peaks, L_{peak}, and the smallest scale contributing to the buoyancy flux, L_{min}, for various stratifications N and grid mesh sizes M

Prandtl numbers, like a thermally stratified water channel, are needed to resolve the Prandtl-number effects.

Both present and past UCSD experiments (e.g. SHV and IHV) have only one external source of turbulent kinetic energy, i.e. the grid. In oceanic and atmospheric flows, complex internal wave fields can act as a source or sink of kinetic energy. Therefore, there might be situations where mixing ($k_1 E_{\rho,w} > 0$) occurs at the smallest scales and restratification ($k_1 E_{\rho,w} < 0$) occurs at the largest scales resulting in a zero net buoyancy flux. Holloway (1983) has also argued that, besides the turbulence, nonlinear internal wave interactions can produce a positive buoyancy flux.

The second important result that can be derived from the spectral content of the buoyancy flux (e.g. figure 4) is the relationship between the Kolmogorov scale L_K and the lengthscale at which $k_1 E_{\rho,w}$ is maximum and the smallest lengthscale contributing to the buoyancy flux. The results from several experiments are summarized in table 2. It is important to notice that scales twice the traditional viscous cutoff of $10L_K$ contribute to most of the vertical mass flux. The large energy-containing scales (of the order of L_t) are responsible for creating large local density gradients by bringing fluid particles of different densities into contact. Then, the viscous scales can smear out these sharp gradients and produce the actual mixing. Independently of the grid mesh size, $k_1 E_{\rho,w}$ is maximal at $L_{peak} \approx 18.5L_K$, while the smallest scale L_{min} contributing to the buoyancy flux appears to depend on the scale of the forcing (in this case the grid mesh size). L_{min} is $2.4L_K$ for $M = 1.905$ cm and $3.4L_K$ for $M = 3.81$ cm. This grid Reynolds-number dependence is very similar to the one noted in (5) between L_O and L_K by IHV. In fact, within experimental uncertainties, L_{min} is one-third of the Ozmidov scale L_O at the downstream location where $(g/\bar{\rho})\overline{\rho w}$ goes to zero.

6. Velocity and density one-dimensional energy spectra

The evolution of the longitudinal and vertical velocity energy spectra behind the vertical rods with stable stratification (R64) is shown in figure 5. The arrow near the lower left corner of figure 5 denotes the Brunt–Väisälä frequency $f_N = 0.14$ Hz (or corresponding wavenumber $k_N = 0.03$ cm^{-1}) below which a saturated two-dimensional internal wave field of slope k^{-2} develops as the kinetic energy of the large turbulent scales is converted into potential energy by the buoyancy forces. A

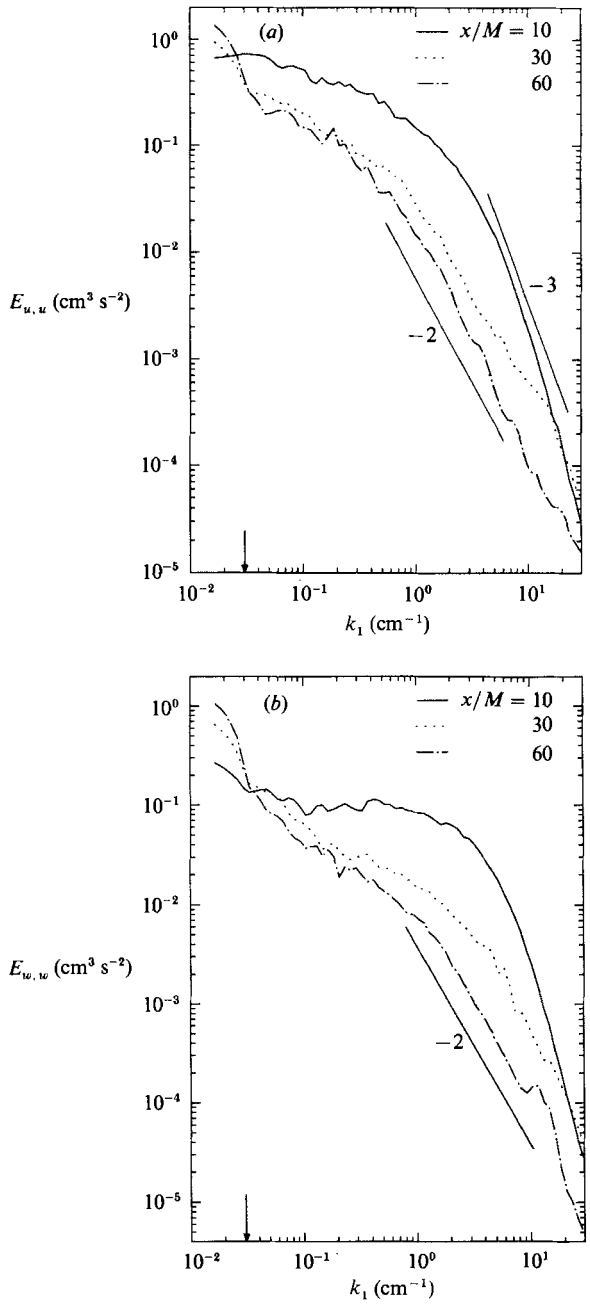

FIGURE 5. Evolution of the velocity power spectra $E_{u,u}$ and $E_{w,w}$ for the first decay ($N = 0.90$ s^{-1}) of R64: (*a*) longitudinal velocity u; (*b*) vertical velocity w.

substantial internal wave field was observed below the Brunt–Väisälä frequency in experiment R64 where a set of vertical rods was used instead of a biplane grid (SHV, IHY). This finding suggests that, in the UCSD water channel, most of the internal waves are generated by the ten interacting jets of the inlet section rather than by the wakes of the horizontal rods in the grids (the vertical rods do not excite internal waves very efficiently).

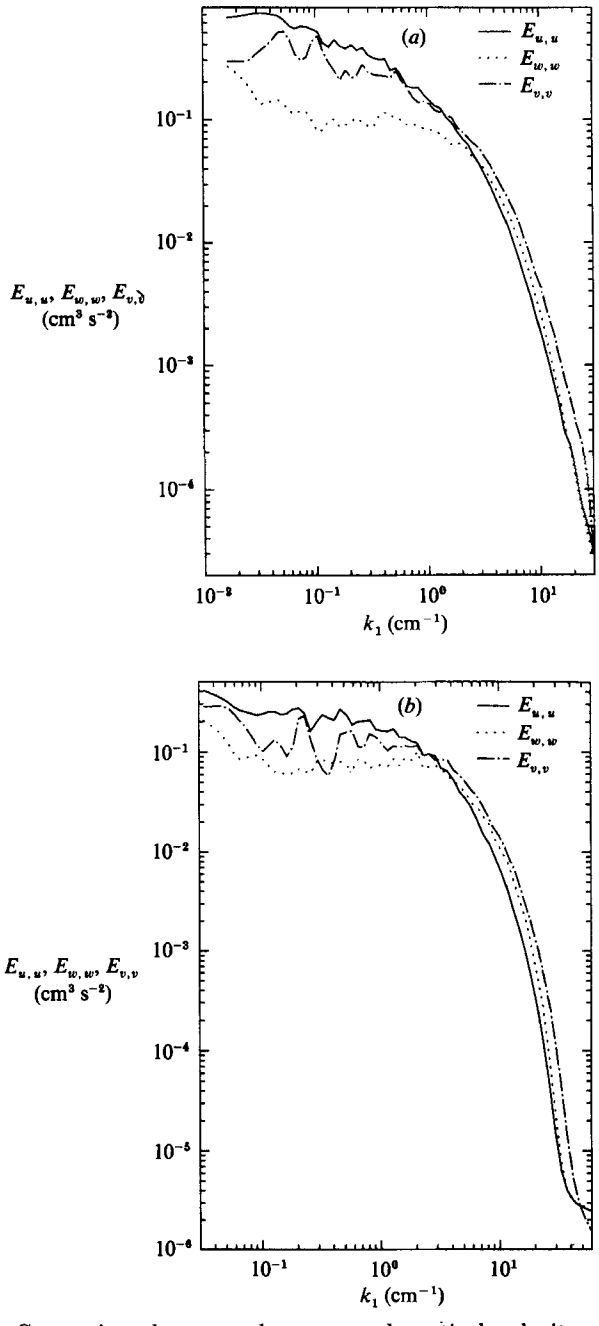

FIGURE 6. Comparison between the measured vertical velocity power spectrum $E_{w,w}$ and the transverse velocity power spectrum $E_{v,v}$ computed from the longitudinal velocity power spectrum $E_{u,u}$ using the isotropic relationship of (13). Data are from: (*a*) R64, $N = 0.90$ s^{-1}, $x/M = 10$ and (*b*) R53, $N = 0.91$ s^{-1}, $x/M = 10$.

Before the onset of buoyancy effects ($x/M = 10$) both velocity spectra exhibit the classical shape of low-Reynolds-number, grid-generated turbulence as observed previously by SHV and IHV. A higher anisotropy due to asymmetry of the vertical rods occurs at the lowest frequencies or equivalently at the largest scales as shown

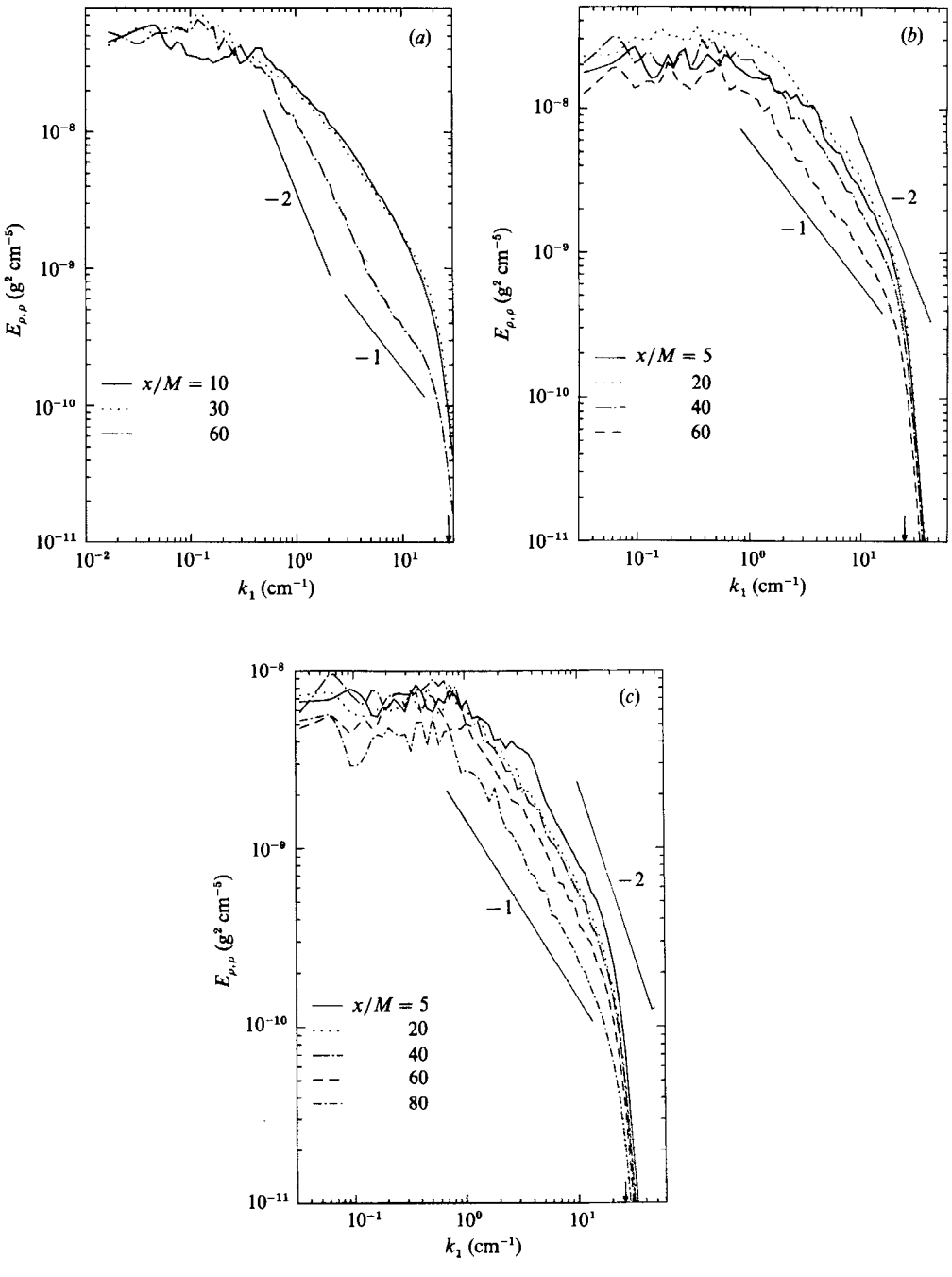

FIGURE 7. Evolution of the density power spectra $E_{\rho,\rho}$: (*a*) first decay of R64, $N = 0.90$ s^{-1}; (*b*) first decay of R53, $N = 0.91$ s^{-1}; (*c*) second decay of R53, $N = 0.65$ s^{-1}. The roll-off of the conductivity probe (−3 dB point) occurs at 25 cm^{-1} as noted by the vertical arrow.

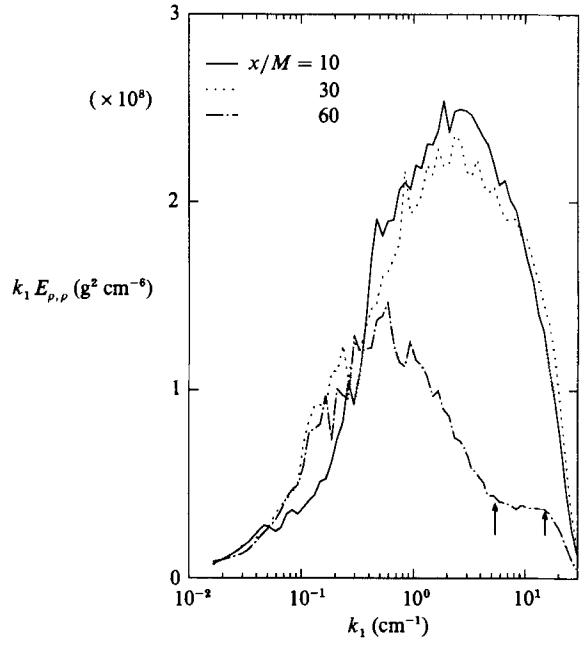

FIGURE 8. Evolution of the density power spectra $k_1 E_{\rho,\rho}$ in area-preserving coordinates for R64, $N = 0.90$ s^{-1}. Note the constant spectral level for $x/M = 60$ between the vertical arrows.

in figure 6 where the transverse velocity power spectrum $E_{v,v}$ has been computed from the longitudinal velocity power spectrum $E_{u,u}$ using the isotropic relationship:

$$E_{v,v}(k_1) = \frac{1}{2}\left(E_{u,u}(k_1) - k_1 \frac{\mathrm{d}}{\mathrm{d}k_1} E_{u,u}(k_1)\right). \tag{31}$$

As seen in figure 6(*a*), the main effect of using vertical rods instead of a biplane grid is to reduce the amount of vertical kinetic energy by a factor of 2 at wavenumbers less than 4 cm^{-1}. In contrast very little suppression of the low-wavenumber part of $E_{w,w}$ is observed behind the small mesh size grid of R53, as shown in figure 6(*b*). The observed difference at the highest wavenumbers between $E_{v,v}$ and $E_{w,w}$ is typical of low-Reynolds-number, grid-generated turbulence.

After the suppression of the buoyancy flux $(g/\bar{\rho})\overline{\rho w}$ $(x/M > 50)$ the longitudinal velocity power spectrum $E_{u,u}$ tends roughly towards a $k^{-2.4}$ shape as in figure 5. This spectral behaviour is rather different from the k^{-3} to k^{-4} predicted by theories of two-dimensional turbulence. No strong evidence of two-dimensionality can be inferred from the shape of the vertical velocity energy spectrum $E_{w,w}$ or the density energy spectrum $E_{\rho,\rho}$ (figure 7). If the buoyancy-dominated turbulence were nearly two-dimensional (in quasi-horizontal sheets or layers) both w and ρ should behave as passive scalars in horizontal planes. Then, their spectra would approach k^{-1} at high wavenumbers. The vertical velocity energy spectra $E_{w,w}$ tends to go as k^{-2} while the density power spectra $E_{\rho,\rho}$ approaches k^{-1}. In one case (R64) there is a small k^{-1} range between 5 cm^{-1} and the conductivity probe roll-off (22.5 cm^{-1}, marked by an arrow in figure 7) at the farthest downstream location $(x/M = 60)$. This k^{-1} range observed at $x/M = 60$ of R64 occurs between wavenumbers $k = 60$ and 160 cm^{-1}, shown by arrows on figure 8. The linear vertical axis of figure 8 shows that the spectral level of $k_1 E_{\rho,\rho}$ between these wavenumbers varies by less than 5%; a

confirmation that it is real. This k^{-1} range has not been consistently observed in all the previous UCSD stratified experiments. Stillinger (1981) observed it behind the small-mesh-size grid ($M = 1.905$ cm), but IHV did not see any strong evidence for a k^{-1} range in the density spectra of either of their two grids.

It should be noted that the spectral shapes predicted by two-dimensional turbulence theories apply to two-dimensional spectra rather than the experimentally measured one-dimensional power spectra. The transformation formula to go from the two-dimensional energy spectrum $E(k)$ to the one-dimensional velocity spectrum $E_{u,u}(k_1)$ (Ogura 1952), where k is the three-dimensional wavenumber:

$$E_{u,u}(k_1) = \frac{1}{\pi}\int_{k_1}^{\infty} E(k)\frac{(k^2-k_1^2)^{\frac{1}{2}}}{k^2}\,\mathrm{d}k \tag{32}$$

or vice versa (Hama 1953):

$$E(k) = -2k^3\frac{\mathrm{d}}{\mathrm{d}k}\left[k\int_k^{\infty}(k_1^2-k^2)^{\frac{1}{2}}\frac{\mathrm{d}}{\mathrm{d}k_1}\left\{\frac{1}{k_1^3}\frac{\mathrm{d}E_{u,u}(k_1)}{\mathrm{d}k_1}\right\}\mathrm{d}k_1\right] \tag{33}$$

are very complex compared with the three-dimensional to one-dimensional relationships because of the reduced symmetries. The corresponding three-dimensional to one-dimensional transformations were derived by Heisenberg (1948):

$$E_{u,u}(k_1) = \frac{1}{2}\int_{k_1}^{\infty}\left(1-\frac{k_1^2}{k^2}\right)\frac{E(k)}{k}\,\mathrm{d}k \tag{34}$$

and Lin (1948):

$$E(k) = k^3\left[\frac{\mathrm{d}}{\mathrm{d}k_1}\left(\frac{1}{k_1}\frac{\mathrm{d}E_{u,u}(k_1)}{\mathrm{d}k_1}\right)\right]_{k_1=k}. \tag{35}$$

The present spectral data were not smooth enough to successfully apply (33) to the one-dimensional spectra. No high-resolution numerical simulations of two-dimensional turbulence are available to show if the slopes of the one- and two-dimensional spectra are significantly different. It should be feasible to investigate the effects of these transformations between one- and three-dimensional spectra using empirical, models spectra; our limited attempts at this were not successful, and numerical computations starting from either a one- or two-dimensional spectrum did not yield convincing results.

However, buoyancy-dominated turbulence in stratified flows like the present experiments should not be expected to be fully two-dimensional for a number of reasons, such as facility limitations, Reynolds-number effects and internal wave-turbulent interactions. First, the physical dimensions of the UCSD water channel and the low Reynolds number do not allow for a wide separation between the energy-containing eddies and the viscous scales, meaning that viscous effects are always important even as the dissipation rate becomes small. The three-dimensional boundary layers on the sidewalls and bottom of the channel could be a sizeable source of production of three-dimensional turbulence at stations downstream of the grid where the original grid-generated turbulence has decayed.

As pointed out by a referee, quasi-two-dimensional eddies rotating in approximately horizontal planes may exist at different elevations in the late stages of the flow, and if the eddies are out of phase with each other, they could induce significant vertical shear (and motions) for the life of the eddies.

Second, and perhaps more important, is the possibility that an initially nearly isotropic, moderate-Reynolds-number turbulent flow subjected to strong buoyancy

forces will lose too much of its kinetic energy to potential energy and dissipation to be able to sustain large two-dimensional eddies. This conclusion is supported by the results of a direct numerical simulation (O. Métais, personal communication, 1987) with similar initial conditions and turbulent Reynolds number. These simulations do not show any clear evidence of two-dimensional turbulence for large decay times (up to ten Brunt–Väisälä periods).

Finally, vertical internal wave motions could significantly alias single-point Eulerian measurements far from the grid, where internal waves have been shown to be the major contributor to vertical kinetic energy (IHV). One could imagine two-dimensional motions confined in quasi-horizontal sheets, subject to vertical displacements and distortion by internal waves. In this case, the appropriate way to measure the spectra would be to either decompose the velocity field into a wave and a vortex component (vertical vorticity) or suppress the internal wave field. Such a wave–vortex decomposition is probably not possible in the laboratory and can only be achieved in direct numerical simulations. Recent numerical simulations of stratified flows (Métais & Herring 1985) show the dominance of the wave–vortex interaction over the vortex–vortex interaction when the initial flow is entirely a random wave field. The developing vortex–vortex interaction (in the vertical direction) has the characteristics of two-dimensional turbulence. Unfortunately Métais & Herring (1985) do not show what the total velocity spectrum looks like.

7. Longitudinal velocity bispectra

If the collapsing, buoyancy-dominated turbulence becomes nearly two-dimensional, the third-order spectrum or bispectrum, a quantity important for the estimation of the energy transfer, may change shape. Bispectra of the longitudinal velocity are defined in terms of the Fourier transforms of the third-order temporal (or spatial, along the direction of the mean flow, when using Taylor's hypothesis of frozen turbulence) correlations. The bispectrum for the longitudinal velocity component u has been defined in §4. This bispectrum can be related to the inertial term in the evolution equation of the longitudinal component of the turbulent kinetic energy in the following manner. Under the experimental conditions in the UCSD water channel, the equation for the evolution of the longitudinal turbulent velocity derived from the Navier–Stokes equations can be approximated by

$$\bar{U}\frac{\partial}{\partial x}\tfrac{1}{2}\overline{u^2}+\overline{uu\frac{\partial u}{\partial x}}+\overline{uv\frac{\partial u}{\partial y}}+\overline{uw\frac{\partial u}{\partial z}}=-\frac{1}{\bar{\rho}}\overline{u\frac{\partial p}{\partial x}}+\nu\overline{u\frac{\partial^2 u}{\partial x_j^2}}. \tag{36}$$

In three-dimensional turbulence, the second to fourth terms of the equation are three of the nine inertial terms contributing to intercomponent transfer of turbulent kinetic energy between different wavenumbers. When the turbulence is isotropic, these nine terms sum to zero. In two-dimensional turbulence (in an (x, y)-plane), the fourth term in (36) is zero and only four inertial terms contribute to the intercomponent energy transfer.

Then

$$\begin{aligned}\overline{uu\frac{\partial u}{\partial x}} &\equiv \int_{-\infty}^{+\infty}\int_{-\infty}^{+\infty}\mathrm{Re}\,[B_{u,\,u,\,(\partial u/\partial x)}(k_1, k_1')]\,\mathrm{d}k_1\,\mathrm{d}k_1' \\ &\equiv -\int_{-\infty}^{+\infty}\int_{-\infty}^{+\infty}(k_1+k_1')\,\mathrm{Im}\,[B_{u,\,u,\,u}(k_1, k_1')]\,\mathrm{d}k_1\,\mathrm{d}k_1'. \end{aligned}\tag{37}$$

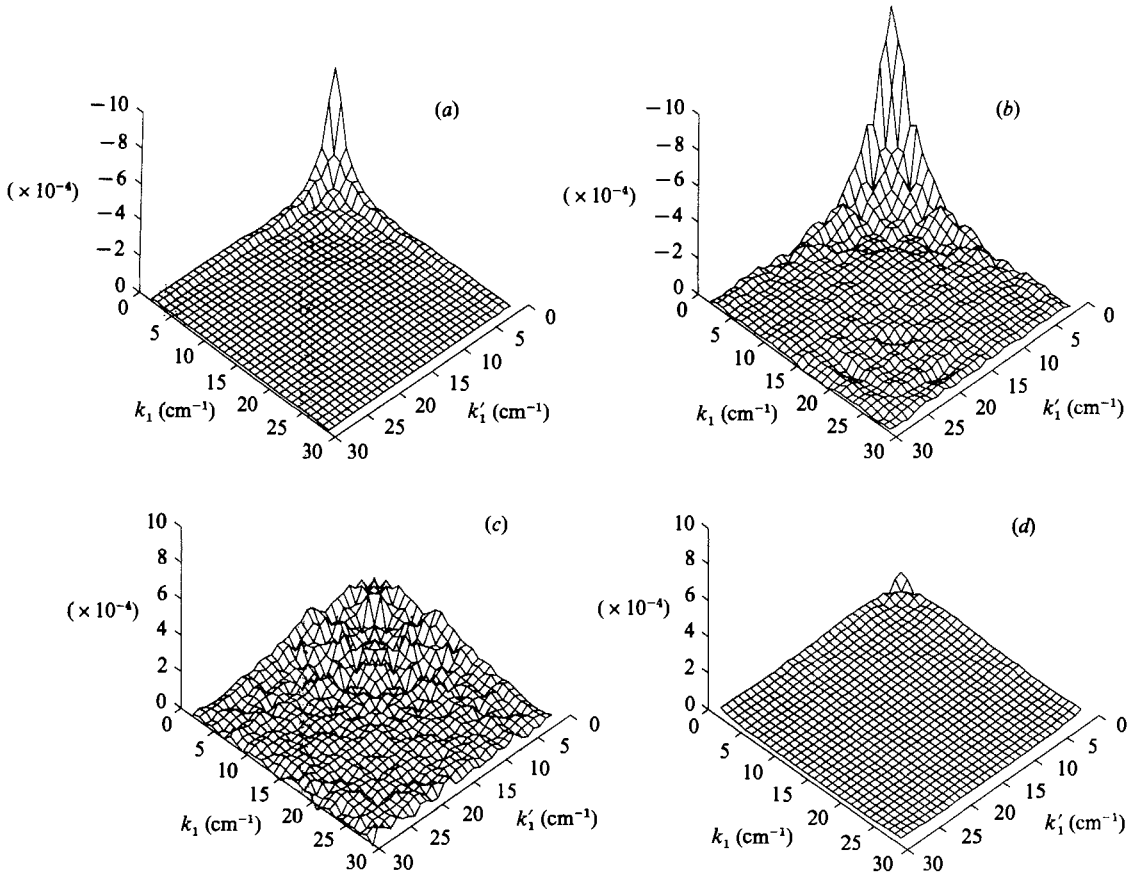

FIGURE 9. Evolution of the imaginary part of the longitudinal velocity bispectra $(k_1+k_1')\,\mathrm{Im}\,B_{u,u,u}(k_1, k_1')$ for (*a*) the unstratified decay (R65), $x/M = 20$; and (*b–d*) the stratified decay (R64): (*b*) $x/M = 10$; (*c*) $x/M = 30$; (*d*) $x/M = 60$. Units for the bispectra are $\mathrm{cm^3\ s^{-3}}$.

For both experiments R64 and R65, 50 records and frequency averaging squares 2.5 Hz (or 0.0625 $\mathrm{cm^{-1}}$) wide provided both good spatial resolution and reasonable statistical smoothing of the bispectral estimates. Each averaging square contained 1600 points whose bispectral values were averaged together over 50 records to yield one bispectral estimate at the midpoint of the averaging square. The statistical resolvability, or ratio of the bispectrum to its local standard deviation, was 3 to 6 for the imaginary part, and less than 3 for the real part of the bispectrum. This result is consistent with previous wind-tunnel measurements (Helland *et al.* 1979) that had a very steady low-intensity turbulent flow, and thus a large number of averaging records (200) could be gathered. Earlier computations with 24 records (R53) showed inadequate resolution (resolvability less than 3 for the imaginary part) of the bispectral estimates. A low resolvability for the real part of the bispectrum should be interpreted to mean that the real part is statistically not distinguishable from zero.

The imaginary parts of the bispectra estimated from measurements taken behind the vertical rods without stratification (R65: $x/M = 20$) and with stratification (R64: $x/M = 10$, 30 and 60) are shown in figure 9. Only the imaginary part of the bispectrum has physical significance for the measurements discussed herein. The real part of the bispectrum should be zero if the motions are isotropic; non-zero

otherwise. The bispectra computed for the unstratified experiment (R65) were similar to bispectra of isotropic grid turbulence (Helland *et al.* 1979; Helland & Rosenblatt 1982; Itsweire & Van Atta 1984) ensuring that no peculiarities due to the experimental set-up were present. The same held true for the bispectrum at $x/M = 10$ in the stratified experiment (R64), since at that location the buoyancy effects were negligible, and the turbulence was nearly isotropic.

The bispectra shown in figure 9 have been multiplied by the sum of the two wavenumbers $(k_1 + k_1')$ in order to obtain the appropriate bispectrum for the one-dimensional energy transfer estimates of the following section (see (22) and (23)). This coordinate system also emphasizes the contributions of the midwavenumbers. Identical vertical scales were chosen in figure 9, albeit with opposite signs for the last two panels, in order to facilitate the comparison between downstream locations. Near the grid (figures 9*a* and 9*b*), the imaginary part of $B_{u,u,u}$ was mostly negative, with a broad peak centred around the zero wavenumber. Wavenumbers below 20 cm^{-1} contributed to the peak. The negative sign of the bispectrum corresponds to an energy cascade from the large scales to the small scales. Where buoyancy affects the dynamics of the large scales of the turbulent flow ($x/M = 30$, figure 9*c*) a reversal in the sign of the bispectrum is observed, indicative of a major change in the energy cascade. Further downstream, where the buoyancy flux has gone to zero and very little vertical mixing occurs ($x/M = 60$, figure 9*d*), the bispectrum is entirely positive, with enhanced contributions from larger wavenumbers. The amplitude of the bispectrum continuously decreases with increasing downstream distance from the grid. As the turbulent kinetic energy decreases, less energy can be transferred among scales. The large values of the bispectrum near either wavenumber axis might be an indication of a strongly non-local energy transfer (Herring 1980).

8. One-dimensional energy transfer

Even though the second-order spectral properties of the collapsed turbulence do not appear to be close to those of two-dimensional turbulence, the collapsed turbulence might still have some of the same properties. One notable property of two-dimensional turbulence is the reverse energy cascade observed in direct Navier–Stokes simulations such as those by Herring *et al.* (1974). In order to investigate the possibility of reverse energy cascade from the small scales to the large scales, estimates of the one-dimensional spectral energy transfer have been made at various stages of the turbulence decay following a method originally outlined by Wilson (1974) and adapted by Van Atta (1979). Our approach is slightly different fom Wilson's, but the final results are the same. Details of his procedure and how his derivations can be interpreted in terms of local and net energy transfer are given in Appendix B.

Equation (23) in §4 gives the algorithm for computing this one-dimensional energy transfer term from the bispectrum of the longitudinal velocity component u. That algorithm required for computing $S(k;l)$ from this equation involves some interpolations since the combinations of wavenumbers expressed in (23) did not coincide with the discrete set of computed bispectral points. Positive values of $S(k;l)$ indicate a net transfer from k to l, while negative values show a net loss of energy from l to k. The cusp-like features in many of the $S(k;l)$-curves near $k \approx l$ are caused by finite-sample (record)-length limitations. This can easily be seen by examining (23) and noting that $S(k;l)$ always requires that at least one term be evaluated near a wavenumber axis $\propto \Delta k$ when $k \approx l$. This was confirmed by using a simple analytical

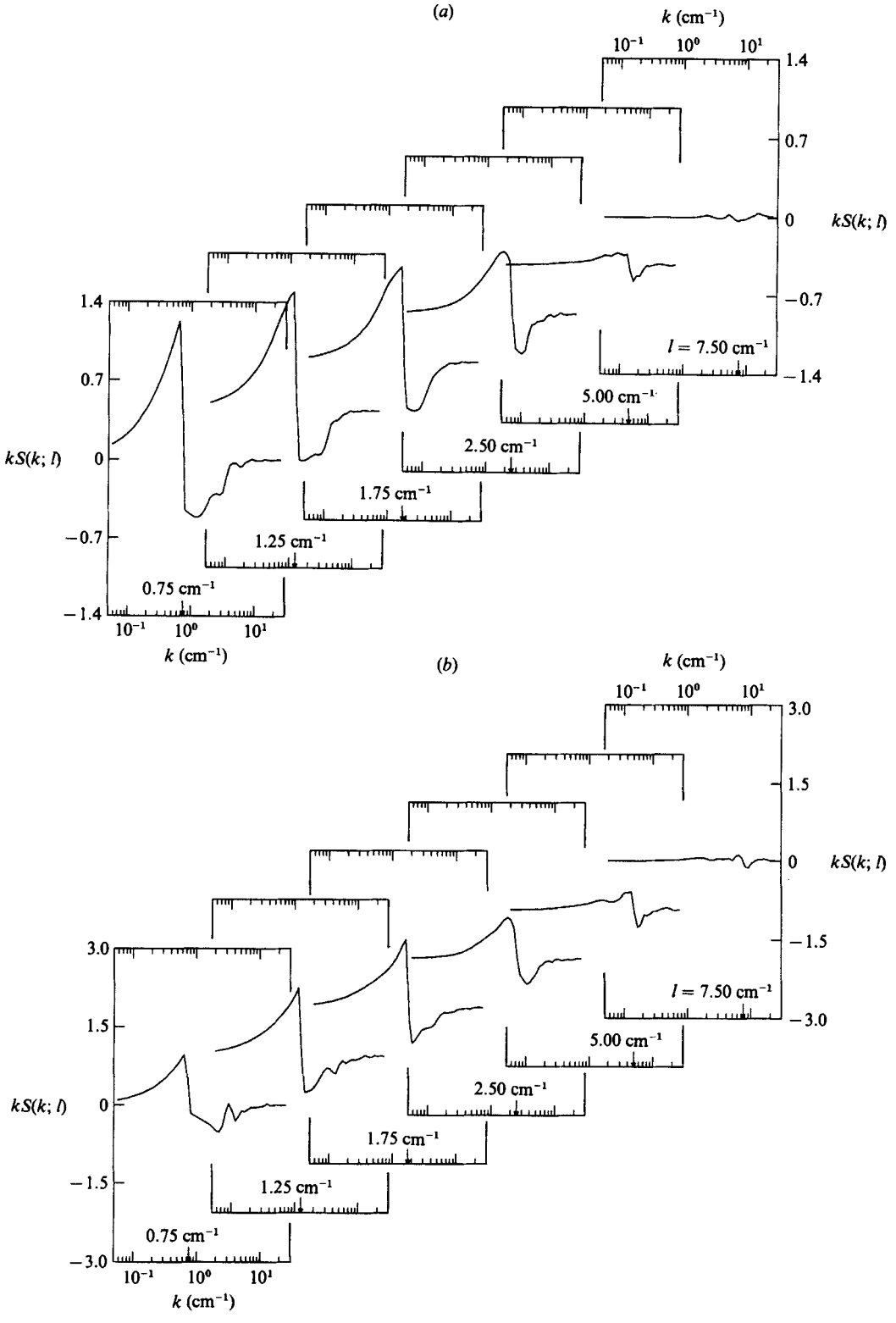

FIGURE 10(*a*, *b*). For caption see facing page.

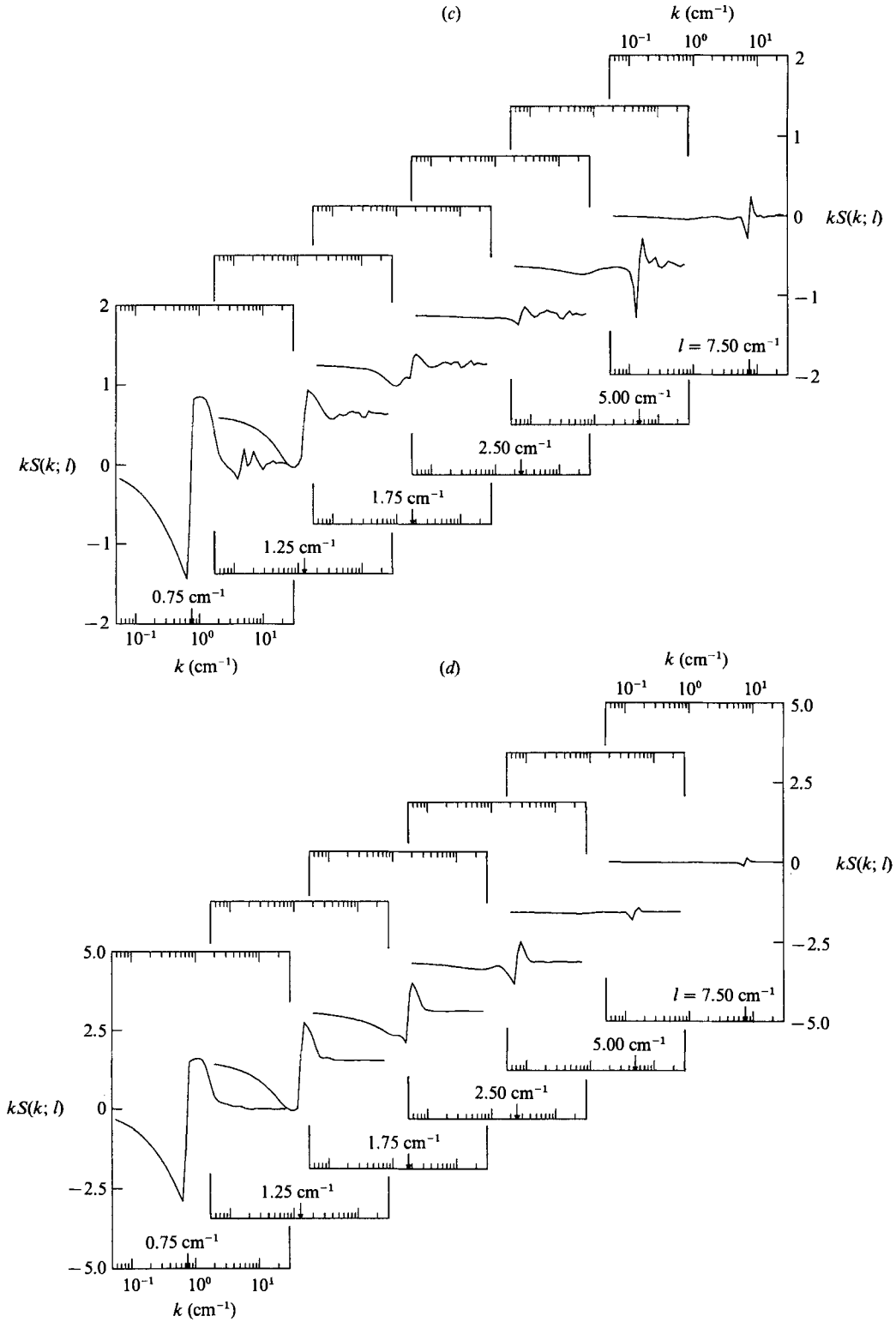

FIGURE 10. Evolution of the one-dimensional longitudinal energy transfer term $S(k;l)$ in area-preserving coordinates for a set of wavenumbers l. The energy transfer terms were computed from the longitudinal velocity bispectra data of figure 9. Shown are (*a*) the unstratified decay (R65), $x/M = 20$; and (*b–d*) the stratified decay (R64): (*b*) $x/M = 10$; (*c*) $x/M = 30$; (*d*) $x/M = 60$.

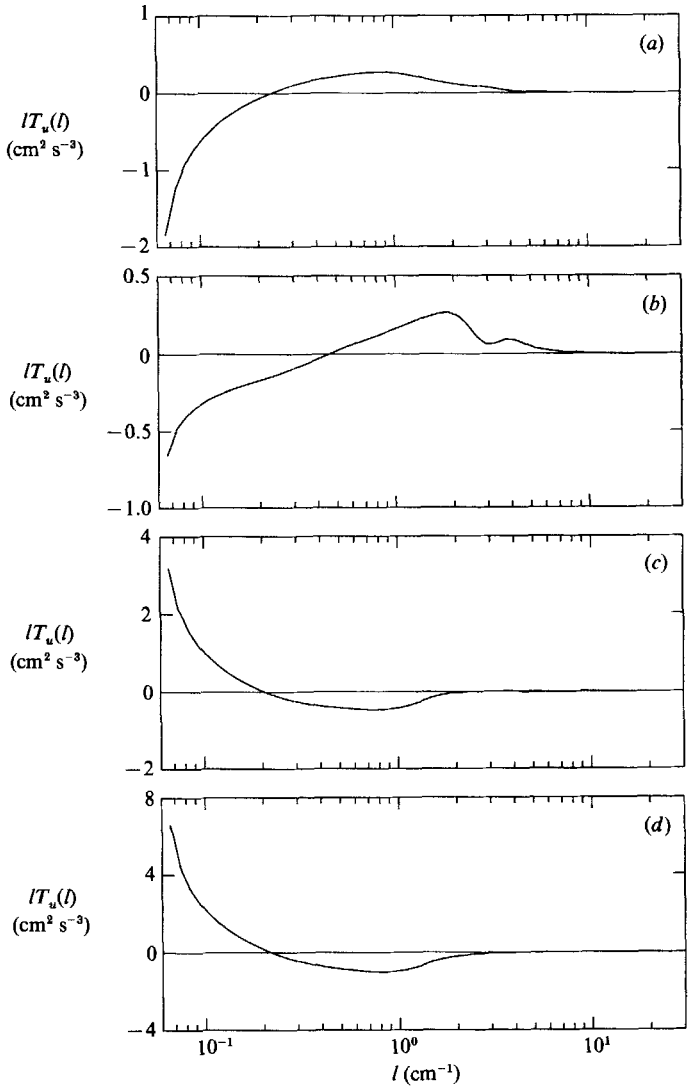

FIGURE 11. Area-preserving plots of the one-dimensional net energy transfer term $T_u(l)$ computed from the longitudinal velocity bispectra data of figure 9. Shown are (*a*) the unstratified decay (R65), $x/M = 20$; and (*b–d*) the stratified decay (R64): (*b*) $x/M = 10$; (*c*) $x/M = 30$; (*d*) $x/M = 60$. Notice the sign reversal when the turbulence is buoyancy-dominated (*c*) or has been suppressed (*d*).

representation of a bispectrum (with well-defined near- and on-axis values) and then computing corresponding $S(k;l)$ values.

The results for the stratified experiment (R64) of figure 10 show that near the grid ($x/M = 10$), the energy is being transferred from small to large wavenumbers. This is the traditional result for three-dimensional turbulence as shown for the unstratified decay of figure 10(*a*) (R65, $x/M = 20$) and other isotropic turbulence experiments (Van Atta 1979; Itsweire & Van Atta 1984). After the onset of buoyancy effects ($x/M = 30$), the energy transfer reverses and energy is then transferred from higher wavenumbers to lower wavenumbers consistent with the behaviour believed to apply for two-dimensional turbulence as shown by the net energy transfer calculations $T(k)$ of Herring *et al.* (1974). The observed energy transfer at $x/M = 30$ is weak and could

indicate that the turbulence is just becoming more two-dimensional than three-dimensional. Further downstream ($x/M = 60$), where no vertical mixing is occurring ($(g/\bar{\rho})\overline{\rho w} = 0$), the magnitude of the reverse energy transfer is four times larger. The energy transfer is largest at the low wavenumbers, which is consistent with a vortex–vortex interaction becoming the dominant mechanism (Métais & Herring 1985).

The transfer terms $S(k;l)$ can be integrated over k for each wavenumber l to give the one-dimensional net energy transfer $T_u(l)$ as shown in §4. By definition, positive values of T_u indicate a net gain of energy at wavenumber l, while negative values show a net energy loss at l. Figure 11 shows how T_u changes when buoyancy effects become important. In all cases the sharp edges of T_u at the lowest wavenumbers are artifacts of the numerical calculations caused by the limited resolution of the bispectral estimates near the zero wavenumber axes. In nearly isotropic, three-dimensional turbulence (R65, $x/M = 20$ and R64, $x/M = 10$, figures 11*a* and 11*b* respectively) the energy cascade is from large to small scales. The energy transfer occurs over a broad band of wavenumbers, all the way to $l = 10$ cm^{-1}. When the turbulence collapses, the net energy transfer reverses from small to large scales and is limited to wavenumbers $l < 3$ cm^{-1}. The magnitude of the energy transfer is also increased several fold.

9. Conclusions

Direct measurements of the buoyancy flux in a density-stratified turbulent flow show the eddy diffusivity model and dissipation techniques can provide reasonable estimates of the buoyancy flux when the turbulence is weakly influenced by buoyancy effects. As buoyancy becomes more important, the mixing efficiency of the flow, and hence the buoyancy flux and eddy diffusivity, decrease rapidly. The spectral representation of the buoyancy flux $(g/\bar{\rho})\overline{\rho w}$, i.e. the real part of the cospectra $E_{\rho,w}$, shows that the smallest scale contributing to the buoyancy flux is about three times the Kolmogorov scale L_K. When the buoyancy flux $(g/\bar{\rho})\overline{\rho w}$ goes to zero, the cospectra $E_{\rho,w}$ is almost identically zero, indicating that no vertical mixing remains at any scales. This result is consistent with the Stillinger *et al.* (1983*b*) and Itsweire *et al.* (1986) use of the buoyancy flux as an indicator for the suppression of three-dimensional turbulence.

After the point of collapse ($(g/\bar{\rho})\overline{\rho w} \approx 0$), the flow appears to be a mixture of small-scale internal waves (wave modes) and two-dimensional turbulence (vortex modes). The slopes of both velocity spectra $E_{u,u}$ and $E_{w,w}$ are different from the slopes predicted by two-dimensional theories of turbulence. Only the density spectra (then a passive scalar) approaches the predicted k^{-1}. These differences in spectral shapes could be attributed to the large internal wave field present in the UCSD experiments. In their direct numerical simulations of stratified flows, Métais & Herring (1985) showed that, when the initial flow was entirely random waves, the wave energy was persistent throughout the evolution of flow, thereby limiting the increase in vortex (two-dimensional turbulence) energy.

Consequently, we turned our attention to the third-order spectrum or bispectrum, thought to be less sensitive to energy transfer among internal waves than within turbulent modes, to see if any reverse energy transfer, a characteristic of two-dimensional turbulence, took place. McComas & Briscoe (1980) noted that for internal waves in the ocean, large (long) internal waves are more energetic but not very nonlinear, and small waves are nonlinear, but not very energetic; thus internal

waves probably do not contribute much to the bispectrum. This is likely to be the case in the laboratory flow as well; we know from spectral measurements that the flow in the late stages of decay is still three-dimensional, but the motions are certainly not the strong, overturning, Kolmogorovian turbulent motions typical of, say, unstratified grid turbulence. We would expect that statistically significant bispectra are a good detector of two- or three-dimensional turbulent motions because of the weakness of the contributions from internal waves. It would also be of great interest to examine, for comparison, energy transfer along the vertical direction.

The one-dimensional inertial transfer term $S(k;l)$ for the longitudinal velocity component was computed from the longitudinal velocity bispectrum $B_{u,u,u}(l,m,k)$ and its behaviour suggests that the traditional energy cascade from the large scales to the small scales reverses when buoyancy effects dominate the dynamics of the flow. The net one-dimensional transfer term $T_u(l)$ also shows the reversal in the energy cascade. The shape of the bispectrum also implies that, after the point of complete collapse ($(g/\bar{\rho})\overline{\rho w} = 0$), the energy transfer is non-local. These results suggest that the collapsed turbulence has some similarity with two-dimensional turbulence. More experiments for other velocity components and under various conditions are needed to determine the universality of these findings. Direct simulations of a similar stratified turbulent flow (Métais & Herring 1989) imply that the initial energy partition between wave and vortex modes could dictate the final state of motion of the fluid.

Preliminary results from this work were presented at the Seventh Symposium on Turbulence and Diffusion, Boulder, Colorado, November 12–15, 1985. This research was supported by the National Science Foundation under Grant OCE82-05946 while both authors were at the University of California, San Diego.

Appendix A. Bispectral symmetries

The bispectral contributions to $S(k;l)$ from each type of interaction come from three sets of regions in the left half-plane as shown in figure 12. The analytical expression for $S(k;l)$ is

$$S(k;l) = -k\,\mathrm{Im}\,[B_{u,u,u}(l,-(l+k),k) = \begin{cases} +k\,\mathrm{Im}\,[B_{u,u,u}(l,-(l-k),-k)], & k<l \\ +k\,\mathrm{Im}\,[B_{u,u,u}(l,+(k-l),-k)], & k>l. \end{cases} \tag{A 1}$$

There are six distinct regions where the bispectra are related through symmetries (Helland *et al.* 1979; Lii & Helland 1981). The type 1 interactions involves bispectra in regions 5 and 6, type 2 interactions have bispectra in regions 3 and 4. Finally, bispectra in regions 1 and 2 contribute to the type 1 interaction. The bispectra in the lower-right quadrant can be mapped into bispectra defined in the upper-right quadrant.

Consider the type 1 interaction first. From Lii & Helland (1981, table 1) a bispectrum in region 5 can be mapped into a bispectrum in region 2 as follows:

$$B_5(\lambda_1,\lambda_2) = B_2(\lambda_1,-\lambda_1-\lambda_2), \tag{A 2}$$

where the subscript i of B_i refers to the wavenumber region of interest. If we make the identification that $\lambda_1 = l$ and $\lambda_2 = -m, m = l+k$ we can write

$$B_5(l,-m) = B_2(l,-l+m) = B_2(l,k). \tag{A 3}$$

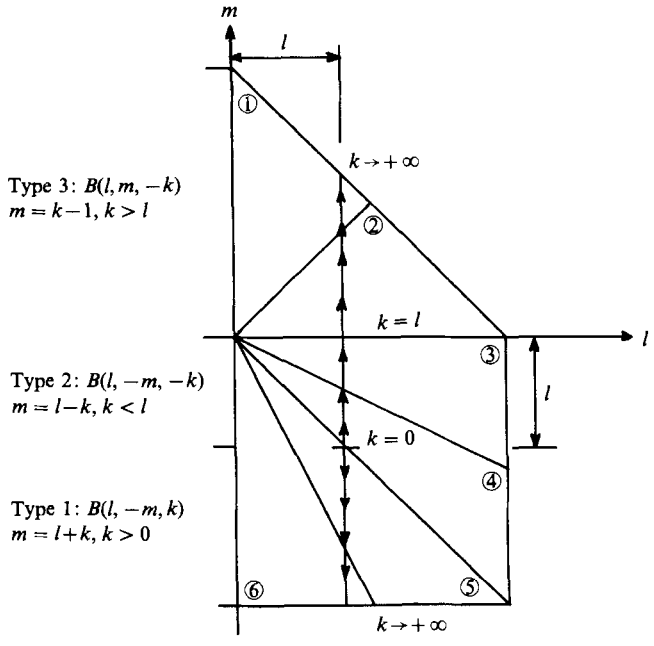

FIGURE 12. Summation domain for $S(k;l)$.

Bispectra in region 6 can be mapped into region 2 using the same relationship:

$$B_6(\lambda_1, \lambda_2) = B_2(-\lambda_1-\lambda_2, \lambda_1) = B_1(\lambda_1, -\lambda_1-\lambda_2). \tag{A 4}$$

Again making the identification $\lambda_1 = l$ and $\lambda_2 = -m, m = l+k$ we can write

$$B_6(l, -m) = B_1(l, k). \tag{A 5}$$

A similar mapping can be used for the bispectra contributing to the type 2 interactions following Lii & Helland (1981):

$$B_3(\lambda_1, \lambda_2) = B_2^*(\lambda_1+\lambda_2, -\lambda_2). \tag{A 6}$$

Again making the identification $\lambda_1 = l$ and $\lambda_2 = -m, m = l-k$ we can write

$$B_3(l, -m) = B_2^*(l-m, +m) = B_2^*(k, l-k). \tag{A 7}$$

Finally bispectra in region 4 can be mapped into region 1 using the same relationship:

$$B_4(l, -m) = B_2^*(l-m, +m) = B_1^*(k, l-k). \tag{A 8}$$

These new transformations for expressing the bispectra in the fourth quadrant in terms of bispectra in the first quadrant (where computations are simpler and faster) can be substituted in (A 1) to get a new expression for $S(k;l)$:

$$S(k;l) = -k\,\mathrm{Im}\,[B_{u,u,u}(l,k)]\begin{cases} -k\,\mathrm{Im}\,[B_{u,u,u}(k,l-k)], & k < l \\ +k\,\mathrm{Im}\,[B_{u,u,u}(l,k-l)], & k > l. \end{cases} \tag{A 9}$$

The expression (A 9) is an operational definition for $S(k;l)$.

Appendix B. Re-examination of Wilson (1974) and Van Atta (1979) analyses

This Appendix re-examines the Fourier analysis of Wilson (1974) and Van Atta's (1979) derivations of $S(k;l)$. We shall show that the end results are the same as those obtained in §4 and are therefore independent of the type of Fourier decomposition used for the velocity field. This result comes to no surprise, but the relationships between the Wilson terms and the quadrant mapping of the bispectrum are somewhat involved.

Wilson (1974) chose to write the Fourier series representation of $u(x,t)$ as

$$u(x) = \sum_k \frac{C_k}{k} \sin(kx+\theta_k), \quad k = 0, 1, 2, \ldots, n-1, \tag{B 1}$$

where θ_k is the phase angle. By expanding the sinus of the sum of two angles, we can rewrite (B 1) in a more usual Fourier series of real coefficients:

$$\begin{aligned} u(x) &= \sum_k \left[\frac{C_k}{k}\sin\theta_k \cos kx + \frac{C_k}{k}\cos\theta_k \sin kx\right] \\ &= \sum_k [A_k \cos kx + B_k \sin kx], \end{aligned} \tag{B 2}$$

where $A_k = (C_k/k)\sin\theta_k$ and $B_k = (C_k/k)\cos\theta_k$. If we rewrite the complex Fourier coefficients of (7) in terms of real and imaginary parts: $F_u(k) = a_k + ib_k$, it is easy to show that $A_k = 2\Delta k a_k$ and $B_k = 2\Delta k b_k$.

Wilson (1974) showed that, within a scale factor, the inertial term of the evolution equation of the individual components resulted from three types of interactions among triads of wavenumbers:

Type 1 $$-\frac{C_l C_m C_k}{4lm}\cos(\theta_l - \theta_m + \theta_k) \quad \text{for} \quad m = l+k, \tag{B 3a}$$

Type 2 $$-\frac{C_l C_m C_k}{4lm}\cos(\theta_l - \theta_m - \theta_k) \quad \text{for} \quad m = l-k, \tag{B 3b}$$

Type 3 $$+\frac{C_l C_m C_k}{4lm}\cos(\theta_l + \theta_m - \theta_k) \quad \text{for} \quad m = k-l. \tag{B 3c}$$

Let's consider the Type 1 interaction defined by (B 3a). Its cosine term can be expanded as follows:

$$\begin{aligned} \cos(\theta_l - \theta_m + \theta_k) = {} & \cos\theta_l \cos\theta_m \cos\theta_k + \cos\theta_l \sin\theta_m \sin\theta_k + \sin\theta_l \sin\theta_m \cos\theta_k \\ & - \sin\theta_l \cos\theta_m \sin\theta_k, \end{aligned} \tag{B 4}$$

so that the Type 1 term can be rewritten as

$$\begin{aligned} -\frac{C_l C_m C_m}{4lm}\cos(\theta_l - \theta_m + \theta_k) = \frac{-1}{4}\Bigg[& \frac{C_l}{l}\cos\theta_l \frac{C_m}{m}\cos\theta_m C_k \cos\theta_k \\ & + \frac{C_l}{l}\cos\theta_l \frac{C_m}{m}\sin\theta_m C_k \sin\theta_k + \frac{C_l}{l}\sin\theta_l \frac{C_m}{m}\sin\theta_m C_k \cos\theta_k - \frac{C_l}{l}\sin\theta_l \frac{C_m}{m}\cos\theta_m C_k \sin\theta_k \Bigg]. \end{aligned} \tag{B 5}$$

We can now substitute the A and B from (B 2) to get

$$-\frac{C_l C_m C_k}{4lm}\cos(\theta_l-\theta_m+\theta_k) = -\tfrac{1}{4}k[B_l B_m B_k + B_l A_m A_k + A_l A_m B_k - A_l B_m A_k]. \tag{B 6a}$$

Similarly the Type 2 and Type 3 terms can be written as

$$-\frac{C_l C_m C_k}{4lm}\cos(\theta_l-\theta_m-\theta_k) = \tfrac{1}{4}k[-B_l B_m B_k + B_l A_m A_k - A_l A_m B_k - A_l B_m A_k], \tag{B 6b}$$

$$+\frac{C_l C_m C_k}{4lm}\cos(\theta_l+\theta_m-\theta_k) = \tfrac{1}{4}k[B_l B_m B_k + B_l A_m A_k - A_l A_m B_k + A_l B_m A_k]. \tag{B 6c}$$

Now that we have expressions for the three types of interactions terms from the Wilson analysis (1974), we need to relate them to the bispectrum as it is computed by the complex Fourier transform analysis of §4. Consider the complex bispectrum

$$\begin{aligned} B_{u,u,u}(l,-m,k) &= F_u(l)\,F_u(-m)\,F_u(k) = F_u(l)\,F_u^*(m)\,F_u(k) \\ &= (a_l+ib_l)(a_m-ib_m)(a_k+ib_k). \end{aligned} \tag{B 7}$$

After expanding the three products and collecting real and imaginary parts, (B 7) becomes

$$\begin{aligned} B_{u,u,u}(l,-m,k) = {} & (a_l a_m a_k + b_l b_m a_k - b_l a_m b_k + a_l b_m b_k) + \mathrm{i}(b_l a_m a_k - a_l b_m a_k \\ & + a_l a_m b_k + b_l b_m b_k) \end{aligned} \tag{B 8a}$$

Similarly, we have

$$\begin{aligned} B_{u,u,u}(l,-m,-k) = {} & (a_l a_m a_k + b_l b_m a_k + b_l a_m b_k - a_l b_m b_k) + \mathrm{i}(b_l a_m a_k - a_l b_m a_k \\ & - a_l a_m b_k - b_l b_m b_k) \end{aligned} \tag{B 8b}$$

and

$$\begin{aligned} B_{u,u,u}(l,m,-k) = {} & (a_l a_m a_k - b_l b_m a_k + b_l a_m b_k + a_l b_m b_k) + \mathrm{i}(b_l a_m a_k + a_l b_m a_k \\ & - a_l a_m b_k + b_l b_m b_k). \end{aligned} \tag{B 8c}$$

We now want to compare the results of expanding the three bispectra of (B 8*a–c*) to the expansions of the Wilson transfer terms of (B 6*a–c*). With the relationships between the various Fourier coefficients, we get

Type 1

$$-\frac{C_l C_m C_k}{4lm}\cos(\theta_l-\theta_m+\theta_k) = -2(\Delta k)^3 k\,\mathrm{Im}\,[B_{u,u,u}(l,-m,k)], \tag{B 9a}$$

where $l-m+k=0$ gives $m=l+k$ with $k>0$.

Type 2

$$-\frac{C_l C_m C_k}{4lm}\cos(\theta_l-\theta_m-\theta_k) = +2(\Delta k)^3 k\,\mathrm{Im}\,[B_{u,u,u}(l,-m,-k)] \tag{B 9b}$$

where $l-m-l=0$ gives $m=l-k$ with $k<l$.

Type 3

$$+\frac{C_l C_m C_k}{4lm}\cos(\theta_l+\theta_m-\theta_k) = +2(\Delta k)^3 k\,\mathrm{Im}\,[B_{u,u,u}(l,m,-k)], \tag{B 9c}$$

where $l+m-k=0$ gives $m=k-l$ with $k>l$. Therefore the three interaction terms of Wilson (1974) are the terms contributing to the one-dimensional transfer terms $S(k;l)$ within a scaling factor of $2(\Delta k)^3$. While the two representations are equivalent, the Fourier series formulation requires the computation of the three transfer terms from a complex, fast Fourier transform using the A and B of (B 6) directly during the averaging process as Wilson did in his analysis. If instead, the averaged, complex bispectrum is computed first, then one cannot escape the use of the symmetry mappings defined in Appendix A, unless, of course, the complex bispectrum is computed for the full right half-plane.

REFERENCES

Britter, R. E., Hunt, J. C. R., Marsh, G. L. & Snyder, W. H. 1983 The effect of stable stratification on turbulent diffusion and the decay of grid turbulence. *J. Fluid Mech.* **127**, 27–44.

Browand, F. K. & Winant, C. D. 1973 Laboratory observations of shear-layer instability in a stratified fluid. *Boundary-Layer Met.* **5**, 67–77.

Champagne, F. H. 1978 The fine-structure of the turbulent velocity field. *J. Fluid Mech.* **86**, 67–108.

Comte-Bellot, G. & Corrsin, S. 1966 The use of a contraction to improve the isotropy of grid-generated turbulence. *J. Fluid Mech.* **25**, 657–682.

Dickey, T. D. & Mellor, G. L. 1980 Decaying turbulence in neutral and stratified fluids. *J. Fluid Mech.* **99**, 13–31.

Dougherty, J. P. 1961 The anisotropy of turbulence at the meteor level. *J. Atmos. Terr. Phys.* **21**, 210–213.

Ellison, T. H. 1957 Turbulent transport of heat and momentum from an infinite rough plane. *J. Fluid Mech.* **2**, 456–466.

Gibson, C. H. 1980 Fossil temperature, salinity and vorticity in the ocean. In *Marine Turbulence* (ed. J. C. T. Nihoul), pp. 221–258. Elsevier.

Gibson, C. H. 1986 Internal waves, fossil turbulence, and composite ocean microstructure spectra. *J. Fluid Mech.* **168**, 89–117.

Gower, J. F. R., Denman, K. L. & Holyer, R. J. 1980 Phytoplankton patchiness indicates the fluctuation spectrum of mesoscale oceanic structure. *Nature* **228**, 157.

Gregg, M. C., D'Asaro, E. A., Shay, T. J. & Larson, N. 1986 Observations of persistent mixing and near-inertial internal waves. *J. Phys. Oceanogr.* **16**, 856–885.

Hama, F. R. 1953 The spectrum of two-dimensional isotropic turbulence. In *Proc. Third Midwestern Conference on Fluid Mechanics, Univ. of Minnesota, Minneapolis*, pp. 427–433.

Head, M. J. 1983 The use of miniature four-electrode conductivity probes for high-resolution measurement of turbulent density or temperature variations in a salt-stratified fluid. Ph.D. thesis, University of California, San Diego.

Heisenberg, W. 1948 On the theory of statistical and isotropic turbulence. *Proc. R. Soc. Lond. A* **195**, 402–406.

Helland, K. N., Itsweire, E. C. & Lii, K. S. 1985 A program for the computation of bispectra with application to spectral energy in fluid turbulence. *Adv. Engng Software* **7**, 22–27.

Helland, K. N., Lii, K. S. & Rosenblatt, M. 1979 Bispectra and energy transfer in grid-generated turbulence. In *Developments in Statistics* (ed. P. R. Krishnaiah), pp. 223–248. North-Holland.

Herring, J. R. 1980 Theoretical calculations of turbulent bispectra. *J. Fluid Mech.* **97**, 193–204.

Herring, J. R. & McWilliams, J. C. 1985 Comparison of direct numerical simulation of two-dimensional turbulence with two-point closure: The effects of intermittency. *J. Fluid Mech.* **153**, 229–242.

Herring, J. R., Orszag, S. A., Kraichnan, R. H. & Fox, D. G. 1974 Decay of two-dimensional homogeneous turbulence. *J. Fluid Mech.* **66**, 5417–5444.

HOLLOWAY, G. 1983 A conjecture relating oceanic internal waves and small-scale processes. *Atmos. Ocean* **21**, 107–122.

HOPFINGER, E., GRIFFITHS, M. & MORY, M. 1983 The structure of turbulence in homogeneous and stratified rotating fluids. *J. Méc. Theor. Appl.* Suppl. (ed. R. Moreau), pp. 21–44.

ITSWEIRE, E. C. 1984 Measurements of vertical overturns in a stably stratified turbulent flow. *Phys. Fluids* **27**, 764–766.

ITSWEIRE, E. C. & HELLAND, K. N. 1985 Turbulent mixing and energy transfer in stably stratified turbulence. In *Seventh Symp. on Turbulence and Diffusion, Boulder, Co.*, pp. 172–175.

ITSWEIRE, E. C., HELLAND, K. N. & VAN ATTA, C. W. 1986 The evolution of grid-generated turbulence in a stably stratified fluid. *J. Fluid Mech.* **162**, 299–338 (referred to as IHV).

ITSWEIRE, E. C. & VAN ATTA, C. W. 1984 An experimental study of the response of nearly isotropic turbulence to a spectrally local disturbance. *J. Fluid Mech.* **145**, 423–445.

KOOP, C. G. & BROWAND, F. K. 1979 Instability and turbulence in a stratified fluid with shear. *J. Fluid Mech.* **93**, 135–159.

KRAICHNAN, R. H. 1971 Inertial-range transfer in two- and three-dimensional turbulence. *J. Fluid Mech.* **47**, 525–535.

LANGE, R. E. 1982 An experimental study of turbulence behind towed biplane grids in a salt-stratified fluid. *J. Phys. Oceanogr.* **12**, 1506–1513.

LIENHARD V, J. H. 1988 The decay of turbulence in a thermally stratified flow. Ph.D. thesis, University of California, San Diego, 400 pp.

LII, K. S. & HELLAND, K. N. 1981 Cross-bispectrum computation and variance estimation. *ACM Trans. Math. Software*, **7**, 284–294.

LII, K. S., HELLAND, K. N. & ROSENBLATT, M. 1982 Estimating three dimensional energy transfer in isotropic turbulence. *J. Time Series Anal.* **3**, 1–28.

LII, K. S., ROSENBLATT, M. & VAN ATTA, C. W. 1976 Bispectral measurements in turbulence. *J. Fluid Mech.* **77**, 45–62.

LIN, C. C. 1948 Remarks on the spectrum of turbulence. *Proc. Symp. Appl. Maths* **1**, 81–86.

LIN, J. T. & PAO, Y. H. 1979 Wakes in stratified fluids. *Ann. Rev. Fluid Mech.* **11**, 317–338.

LIN, J. T. & VEENHUIZEN, S. D. 1975 Measurements of the decay of grid-generated turbulence in a stratified fluid. *Flow Research Note No.* 85, 32 p.

MCCOMAS, C. H. & BRISCOE, M. G. 1980 Bispectra of internal waves. *J. Fluid Mech.* **9**, 205–213.

MÉTAIS, O. 1985 Influence of stable stratification on three-dimensional isotropic turbulence. In *Turbulent Shear Flow V* (ed. J. L. Lumley), p. 22.27. Springer.

MÉTAIS, O. & HERRING, J. R. 1985 Numerical and theoretical results relating to mesoscale turbulence. In *Seventh Symposium on Turbulence and Diffusion*, Boulder, Co, 188–191.

MÉTAIS, O. & HERRING, J. R. 1989 Numerical simulations of freely evolving turbulence in stably stratified fluids. *J. Fluid Mech.* **202**, 117–148.

MONTGOMERY, R. D. 1974 An experimental study of grid turbulence in a thermally stratified flow. Ph.D. thesis, University of Michigan, 145 pp.

OAKEY, N. S. 1982 Determination of the rate of dissipation of turbulent kinetic energy from simultaneous temperature and velocity shear microstructure measurements. *J. Phys. Oceanogr.* **12**, 256–271.

OGURA, Y. 1952 The structure of two-dimensionally isotropic turbulence. *J. Met. Soc. Japan*, **30**, 59–64.

ORSZAG, S. A. 1974 *Statistical Theory of Turbulence, Les Houches Summer School on Physics.* Gordon & Breach.

OSBORN, T. R. 1980 Estimates of the local rate of vertical diffusion from dissipation measurements. *J. Phys. Oceanogr.* **10**, 83–89.

OZMIDOV, R. V. 1965 On the turbulent exchange in a stably stratified ocean. *Atmos. Ocean. Phys.* **8**, 853–860.

PEARSON, H. J., PUTTOCK, J. S. & HUNT, J. C. R. 1983 A statistical model of fluid-element motions and vertical diffusion in a homogeneous stratified turbulent flow. *J. Fluid Mech.* **129**, 219–249.

RILEY, J. J., METCALFE, R. W. & WEISSMAN, M. A. 1981 Direct numerical simulations of

homogeneous turbulence in density stratified fluids. In *Nonlinear properties of internal waves, La Jolly Institute, AIP Conf. Proc.* (ed. B. J. West), vol. 76, pp. 79–112.

ROHR, J. J., ITSWEIRE, E. C. & VAN ATTA, C. W. 1984 Mixing efficiency in stably stratified decaying turbulence. *J. Geophys. Astrophys. Fluid Dyn.* **29**, 221–236.

ROHR, J. J. & VAN ATTA, C. W. 1987 Mixing efficiency in stably stratified growing turbulence. *J. Geophys. Res.* **92**, 5481–5488.

SIRIVAT, A. & WARHAFT, Z. 1983 The effect of a passive cross-stream temperature gradient on the evolution of temperature variance and heat flux in grid turbulence. *J. Fluid Mech.* **128**, 323–346.

SOMMERIA, J. 1983 Two-dimensional behaviour of MHD fully developed turbulence ($Rm \gg 1$). *J. Méc. Theor. Appl.*, Suppl. (ed. R. Moreau), pp. 169–190.

SOMMERIA, J. & MOREAU, R. 1982 Why, how, and when, MHD turbulence becomes two-dimensional. *J. Fluid Mech.* **118**, 507–518.

STEWART, R. W. 1969 Turbulence and waves in a stratified atmosphere. *Radio Sci.* **4**, 1289–1278.

STILLINGER, D. C. 1981 An experimental study of the transition of grid turbulence to internal waves in a salt-stratified water channel. Ph.D. thesis, University of California, San Diego.

STILLINGER, D. C., HEAD, M. J., HELLAND, K. N. & VAN ATTA, C. W. 1983*a* A closed-loop gravity-driven water channel for density-stratified shear flows. *J. Fluid Mech.* **131**, 73–90 (referred to as SHV).

STILLINGER, D. C., HELLAND, K. N. & VAN ATTA, C. W. 1983*b* Experiments on the transition of homogeneous turbulence to internal waves in a stratified fluid. *J. Fluid Mech.* **131**, 91–122 (referred to as SHV).

VAN ATTA, C. W. 1979 Bispectral measurements in turbulence computations. In *Proc. 6th Intl Conf. on Numerical Methods in Fluid Dynamics, Tsibili, June 1978* (ed. H. Cabannes, M. Holt & V. V. Rusanov). Lecture Notes in Physics, vol. 90, pp. 530–536. Springer.

VAN ATTA, C. W., HELLAND, K. N. & ITSWEIRE, E. C. 1984 The influence of stable stratification on spatially decaying vertically homogeneous turbulence. In *Proc. IUTAM Symposium on Turbulence and Chaotic Phenomena in Fluids, Sept. 1983, Kyoto, Japan* (ed. T. Tatsumi), pp. 519–523, North-Holland.

WEINSTOCK, J. 1978 Vertical turbulent diffusion in a stably stratified fluid. *J. Atmos. Sci.* **35**, 1022–1027.

WILSON, J. R. 1974 Some observed statistical properties of small-scale turbulence. Ph.D. Thesis, University of British Columbia.

YEH, T. T. & VAN ATTA, C. W. 1973 Spectral transfer of scalar and velocity fields in heated grid turbulence. *J. Fluid Mech.* **58**, 233–261.